

Hybrid Two-level MCMC with Deep Learning Surrogates for Bayesian Inverse Problems

Juntao Yang^a, Jeff Adie^a, Simon See^a, Adriano Gualandi^{b,c}, Gianmarco Mengaldo^d

^a*NVIDIA AI Technology Center, Singapore,*

^b*University of Cambridge, United Kingdom,*

^c*Istituto Nazionale di Geofisica e Vulcanologia, Italy,*

^d*National University of Singapore, Singapore,*

Abstract

Bayesian inverse problems arise in various scientific and engineering domains, and solving them can be computationally demanding. This is especially the case for problems governed by partial differential equations, where the repeated evaluation of the forward operator is extremely expensive. Recent advances in Deep Learning (DL)-based surrogate models have shown promising potential to accelerate the solution of such problems. However, despite their ability to learn from complex data, DL-based surrogate models generally cannot match the accuracy of high-fidelity numerical models, which limits their practical applicability. We propose a novel hybrid two-level Markov Chain Monte Carlo (MCMC) method that combines the strengths of DL-based surrogate models and high-fidelity numerical solvers to solve Bayesian inverse problems governed by partial differential equations. The intuition is to leverage the inference speed of a DL-based surrogate model as the base chain, and correct its errors using a limited number of high-fidelity numerical model evaluations in a correction chain; hence its name hybrid two-level MCMC method. Through a detailed theoretical analysis, we show that our approach can achieve the same accuracy as a pure numerical MCMC method while requiring only a small fraction of the computational cost. The theoretical analysis is further supported by several numerical experiments on the Poisson, reaction-diffusion, and Navier-Stokes equations. The proposed hybrid framework can be generalized to other approaches such as the ensemble Kalman filter and sequential Monte Carlo methods.

Keywords: Markov Chain Monte Carlo, Deep Learning, Bayesian Inverse

1. Introduction

Inverse problems arise in various fields of applied science, including design optimization in engineering, seismic inversion in geophysics, and data assimilation in weather forecasting [29]. The behavior of these systems is described by a mathematical model that frequently consists of a system of partial differential equations that depends on a set of inputs and parameters. Inverse problems involve determining the inputs or parameters of the mathematical model based on observations or partial observations of the model solution. The mathematical model, in the context of inverse problems, is also known as the forward problem, and it is typically expressed as

$$y = \mathcal{G}(z), \tag{1}$$

where \mathcal{G} is the forward operator (also referred to as the forward map), z represents the inputs or parameters, and y are the observed data defined in Equation (1).

The objective of an inverse problem is to identify the inputs or parameters z , or some quantity of interest that depends on z . Optimization techniques, such as least squares optimization, are commonly employed to solve inverse problems [2, 46]. However, inverse problems are often ill-posed, meaning they may lack uniqueness, stability, or the existence of a solution.

To address the challenges related to ill-posedness, Tikhonov regularization is frequently used [2, 29]. Although the incorporation of Tikhonov regularization might initially seem arbitrary, it can be explicitly interpreted from a Bayesian perspective as a prior distribution. This connection bridges the optimization approach with the probabilistic Bayesian framework, where data are considered as observations subject to noise. In this context, a noise term η is added to the forward operator defined in Equation (1) to account for observational noise.

$$y = \mathcal{G}(z) + \eta. \tag{2}$$

In this work, we adopt a Bayesian approach to inverse problems, such as the one in equation (2), leveraging Bayes' rule to account for uncertainties in both the model and observations.

The central idea of the Bayesian approach is to combine prior knowledge about inputs and parameters z with the information provided by the observed

data y . This step is accomplished by using the likelihood of the data given the parameters $P(y|z)$ and a prior distribution $P(z)$ from our prior knowledge. The Bayes' theorem (also referred to as Bayes' rule) then allows the computation of a posterior distribution, which reflects the updated beliefs about the unknowns after observing the data, which is commonly written as $P(z|y) = P(y|z)P(z)/P(y)$. To be more general, Bayes' theorem is often expressed formally with measure-theoretic terms from the mathematical framework of the Radon-Nikodym theorem, such that probability masses or densities over real numbers can be extended to probability measures over any arbitrary sets [7]. In this framework, the posterior measure and the prior measure are related through the Radon-Nikodym derivative [45].

Bayesian inverse problems can be finite- [2], or infinite-dimensional [45]. The former usually arises in the context of parameter estimation, whereby a finite set of parameters is of interest. The latter instead arises in the context of full-field inversion of partial differential equations (PDE) problems, where infinite-dimensional functions are of interest. In our paper, we adopt the Bayes theorem in measure-theoretic terms, which is compatible with the infinite-dimensional setup.

Typically solving Bayesian inverse problems leads to the repeated solution of the forward problem in equation (2). For example, to solve PDE-based (i.e. infinite-dimensional) Bayesian inverse problems, it is necessary to discretize the continuous PDE problem via a suitable numerical method, such as the finite element method [8] or the finite volume method [32]. This often leads to a high-dimensional linear system of equations, that are extremely expensive computationally. These computationally expensive high-dimensional linear systems, in turn, need to be solved several times to approximate the posterior distribution, making the problem intractable due to the curse of dimensionality.

Recent developments in deep learning (DL) have provided a possible pathway to accelerate the solution of Bayesian inverse problems. In particular, DL-based models (i.e., deep neural networks) can be used as surrogate models to substitute the computationally expensive high-dimensional linear system of equations that arise when numerically discretizing the continuous PDE problem. Two of the critical advantages of DL-based surrogates are their fast differentiability (thanks to automatic differentiation) and fast inference properties. The first feature makes DL-based surrogates an excellent candidate for solving Bayesian inverse problems using deterministic methods, such as variational methods; see, e.g. [36]. Variational methods typically

lead to finding the maximum a posteriori (MAP) with optimization techniques. Gradient-based optimization such as gradient descent and L-BFGS is one family of the most used optimization techniques for variational methods. Gradients can be easily computed by automatic differentiation from a differentiable DL-based surrogate model, which makes the DL-based surrogate model a great fit. The second feature makes them an excellent candidate for sampling-based statistical methods, such as Markov Chain Monte Carlo and ensemble Kalman filter. These sampling techniques approximate the posterior distribution through Monte Carlo samples, which typically converge at a slow rate of $1/\sqrt{N}$ (N being the number of samples). In this case, the fast inference speed of DL-based surrogates can be utilized to dramatically accelerate sampling procedures.

In the literature, several works explored the use of DL-based models for inverse problems. For example, physics-informed neural networks (PINNs) have demonstrated their ability to solve parameterized PDEs; feature that can be used for finite-dimensional inverse problems, such as design optimization [42]. Neural operators have shown that they can learn linear and non-linear mappings between function spaces [35]; hence, they are a promising category of DL-based surrogates for infinite-dimensional inverse problems (e.g. [33]). Indeed, the fast inference properties of neural operators make them extremely competitive for high-dimensional problems with respect to more traditional surrogate models, such as generalized polynomial chaos and Gaussian processes. These recent advances have made the solution of otherwise intractable inverse problems a real possibility.

However, despite the advantages of DL-based surrogate models for inverse problems, there are still some key areas that need to be addressed. Namely, a complete mathematical framework to estimate the error bounds of a deep neural network model is still missing. The expected error bounds (also referred interchangeably as error estimates) consist of three components: approximation error, optimization error, and generalization error [28]. While universal approximation theorems exist [10, 31], together with the expressivity analysis of neural networks (that depends on the number of layers and nodes provided) [40, 48], these only address the approximation error. A large body of literature attempts to address the optimization error by investigating the landscape of non-convex loss functions as well as the optimization process by stochastic gradient [1, 13, 27, 28]. Some works also attempt to quantify the generalization error [28]. However, a general theory is still lacking as most existing analyses make several simplifying assumptions that do not hold for

practical problems.

Because of this lack of theoretical error framework, DL-based models are commonly treated as a black-box, and the expected error bounds are empirically estimated, noting that more data available could lead to better accuracy (property known as the power law) [3, 19].

In the context of Bayesian inverse problems, the lack of a rigorous theoretical framework on DL models' error bounds hinders the adoption of DL surrogates in critical applications, where a desired error estimated a priori may be required. In fact, in Bayesian inverse problems, a naive replacement of a high-fidelity numerical PDE solver with a DL-based surrogate will lead to propagation of the error of the surrogate to the posterior distribution [9]. For instance, in the context of MCMC methods, that sample the posterior distribution with an ergodic Markov Chain generated by a given algorithm (e.g., the Metropolis-Hasting algorithm [6]), the error on the posterior depends on the surrogate error shown in Section 2.2.2.

Therefore, in order to make the DL-based surrogate model practically useful in solving Bayesian inverse problems, e.g., using MCMC methods, the posterior error induced by the DL surrogate needs to be contained to a given a priori threshold, an aspect that is still lacking and that represents a key gap in the literature.

In this work, we focus on MCMC methods that are among the most widely adopted methods for solving Bayesian inverse problems, given their ability to handle high-dimensional problems and their embedded uncertainty estimates. However, they have a critical issue: they are extremely expensive computationally. To address this issue, we propose a new MCMC method to solve Bayesian inverse problems that we named *two-level hybrid MCMC approach*. The new method leverages the fast inference properties of DL surrogates to accelerate the MCMC method, while also using a high-fidelity numerical model for accuracy. The latter aspect allows for a priori theoretical error estimates that are typically not readily available when using DL surrogates.

Our *two-level hybrid MCMC approach* uses a DL-based surrogate model to obtain a base MCMC chain with a large number of samples (leveraging the fast inference speed of the DL surrogate). A short correction MCMC chain is then generated to sample the differences between the high-fidelity numerical model and the DL-based surrogate model. This is done to correct for the bias introduced by the surrogate as shown in Fig 1.

We provide a detailed theoretical analysis, showing that the new method

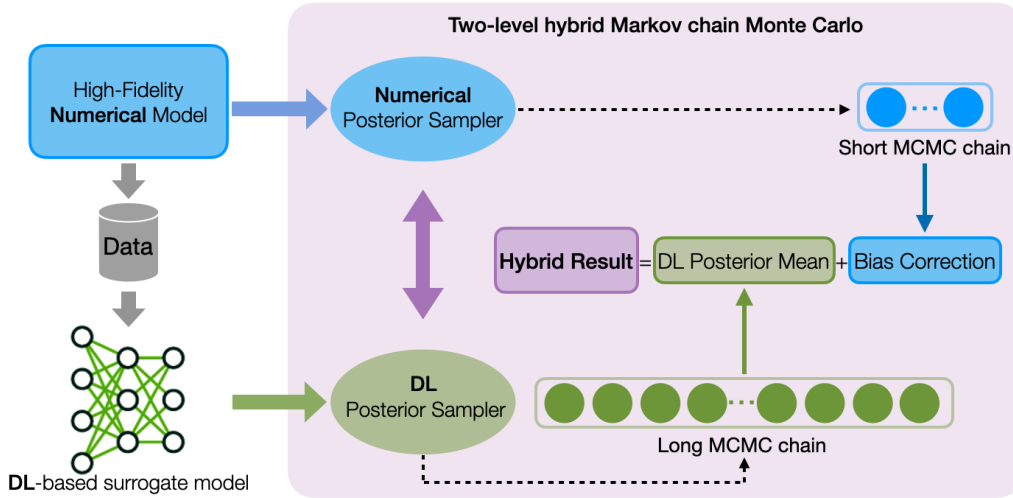


Figure 1: Hybrid two-level MCMC

has the same a priori error bound $\mathcal{O}(h)$ as a plain MCMC chain that uses a high-fidelity numerical model (discretized at a known mesh size equal to h). However, our method requires a small fraction of the computational cost necessary to run a plain MCMC chain with a high-fidelity numerical model.

We complement the theoretical findings with numerical experiments on elliptic, reaction-diffusion, and fluid dynamics problems. The numerical results support the theoretical findings and highlight how the new method provides a lightweight DL-based surrogate alternative to existing MCMC approaches, with rigorously defined a priori error bounds. The latter aspect closes the gap in the literature regarding the lack of rigorous error bounds when using DL-based surrogates, and constitutes an important milestone for the fast solution of Bayesian inverse problems via deep learning. The rest of the paper is organized as follows. Section 2, introduces the Bayesian inverse problem setup (Section 2.1), the approximation of the forward problem (Section 2.2), and the new hybrid two-level MCMC for a uniform prior (Section 2.3), noting that the Gaussian prior case is presented in Appendix A. Section 3 shows the numerical experiments that validate the theoretical estimates provided in Section 2. Section 4 draws some closing remarks, including limitations and future work.

2. A new approach to accelerate Bayesian inversion

2.1. Bayesian inverse problem setup

To present our new approach, we first introduce the theoretical background of Bayesian inverse problems. We consider inverse problems governed by a forward mathematical model as the one defined in equation (2), where the underlying system is constituted of PDEs. More formally, the PDE-based forward model predicts the states u provided the inputs/parameters $\mathbf{z} = \{z_1, z_2, \dots, z_n\}$. In order to introduce the problem setup based on Equation (2), we need to define the inputs/parameters \mathbf{z} , the forward operator (or forward map) $\mathcal{G}(\mathbf{z})$, and the observational noise η .

We start by defining the inputs/parameters \mathbf{z} . These represent a finite number of constants or functions within the governing equations, or the coefficients associated with the spectral expansion of a random field defining the initial conditions or forcing terms. For example, \mathbf{z} can be the Lamé constants of the material in the elasticity equation of solid mechanics [5], the coefficient of the Karhunen–Loève expansion of the porosity random field in the subsurface flow model [12], or the initial condition and random forcing in the Navier-Stokes equations [11]. In many practical applications, the following truncated Karhunen–Loève expansion of a random field K is commonly used,

$$K(z) = \bar{K} + \sum_{j=1}^n z_j \psi_j, \quad (3)$$

where \bar{K}, ψ_j are functions in L^∞ . For simplicity, hereafter we name \mathbf{z} as the *parameters* of the forward problem, without lacking generality.

In the context of Bayesian inverse problems, we need to define the *prior* probability distribution for the parameters \mathbf{z} . To this end, we consider a uniform prior, where z_i in \mathbf{z} is uniformly distributed within $[-1, 1]$. By denoting \mathcal{B} the Borel σ -algebra, we define a measurable space (U, Θ) , where Θ is a σ -algebra on U , defined as $\Theta = \bigotimes_{j=1}^n \mathcal{B}([-1, 1])$, and $U = [-1, 1]^n$ is the parameter space. Together with the prior measure $\gamma = \bigotimes_{j=1}^n \frac{dz_j}{2}$ on the measurable space (U, Θ) , we have the complete probability space (U, Θ, γ) .

With the prior measure of \mathbf{z} defined, we focus on the forward operator (or map) \mathcal{G} . Within the framework just introduced, the forward operator can be written as follows,

$$\mathcal{G} : U \rightarrow \mathbb{R}^k \quad \forall \mathbf{z} \in U; \quad \mathcal{G}(\mathbf{z}) = (\mathcal{F}_1(u(\mathbf{z})), \mathcal{F}_2(u(\mathbf{z})), \dots, \mathcal{F}_k(u(\mathbf{z}))), \quad (4)$$

where $u(\mathbf{z}) \in V$ is the state solution of the forward PDEs which depends on the input \mathbf{z} , and $\mathcal{F}_i(\cdot), i = 1, 2, \dots, k$ are k continuous bounded linear functionals. V is a suitable vector space, e.g. a Sobolev space, which depends on the specific equations and problem. \mathcal{F} is included in the forward operator to better reflect real-world problems, where real-world observations are usually discrete and sparse while the state solutions of a PDE system are typically continuous functions. For example, in the context of weather data assimilation, \mathcal{F} is known as the observation operator [44]. In order to frame our Bayesian problem and guarantee the existence of the posterior, we need to formulate a key assumption on the forward operator \mathcal{G} .

Assumption 2.1. *The forward operator $\mathcal{G}(z) : U \rightarrow \mathbb{R}^k$ is a continuous map from the measurable space (U, Θ) to $(\mathbb{R}^k, \mathcal{B}(\mathbb{R}^k))$.*

Assumption 2.1 is valid for most PDE-constrained systems, and it leads to the existence of the posterior in Bayesian inverse problems. Proofs of Assumption 2.1 for elliptic and parabolic equations can be found in [22, 24], while the proofs for the elasticity and Navier-Stokes equations can be found in [11, 45].

We finally define the observational noise, η . We assume it to be Gaussian and independent of the parameters \mathbf{z} . Therefore, η is a random variable with values in \mathbb{R}^k and it follows a normal distribution $\mathcal{N}(0, \Sigma)$, where Σ is a known $k \times k$ symmetric positive covariance matrix.

Having defined the parameters \mathbf{z} , the forward operator \mathcal{G} , and the observational noise η , along with the measurable space (U, Θ) , and the prior distribution of the parameters γ , we now show the existence of the posterior, which we denote by γ^y . This is possible thanks to Assumption 2.1 that leads to γ^y being absolutely continuous with respect to the prior γ . The posterior probability measure is defined through the Radon-Nikodym derivative

$$\frac{d\gamma^y}{d\gamma} \propto \exp(-\Phi(z; y)), \quad (5)$$

where Φ is known as the potential function, for example with Gaussian noise assumption, $\Phi(z, y) = \frac{1}{2}|y - \mathcal{G}(z)|_{\Sigma}^2$. Detailed proof of equation (5) can be found in [45].

The last step to fully setup the framework is to show that the posterior measure is well-posed. This can be achieved following the results in [11, 21, 45], that details how the posterior measure is Lipschitz continuous with

respect to the data under a certain distance metric. Specifically, for every $r > 0$ and $y, y' \in \mathbb{R}^d$ with $|y|_\Sigma, |y'|_\Sigma \leq r$, there exists $C = C(r) > 0$ such that

$$d_H(\gamma', \gamma'') = \left(\frac{1}{2} \int_U \left(\sqrt{\frac{d\gamma'}{d\gamma}} - \sqrt{\frac{d\gamma''}{d\gamma}} \right)^2 d\gamma \right)^{\frac{1}{2}} \leq C(r) |y - y'|_\Sigma, \quad (6)$$

where γ' and γ'' are two measures on U , which are absolutely continuous with respect to the measure γ , and where we chose as a distance metric the Hellinger distance d_H . The latter was chosen to facilitate various proofs related to our new hybrid two-level MCMC approach, leading to Theorem 2.1, in Section 2.3.

We note that the setup considered uses a uniform prior for the sake of simplicity. However, we can also work with a Gaussian setup, e.g. $U = \mathbb{R}^k$, $\Theta = \bigotimes_{j=1}^n \mathcal{B}(\mathbb{R})$, and $\gamma = \bigotimes_{j=1}^n \mathcal{N}(0, 1)$.

2.2. Approximation of the forward problem

A particularly expensive task in the Bayesian inverse problem setup introduced in Section 2.1 is the solution of the forward problem, especially when the forward operator \mathcal{G} is constituted of PDEs. We distinguish two cases: (i) when the PDEs are approximated and solved via traditional numerical methods (e.g., FEM or others), also referred to as high-fidelity numerical models/solvers, and (ii) when the PDEs are solved via DL surrogates. We detail these two cases next, where, leveraging the results highlighted in Section 2.1, we derive theoretical error estimates for each case, and make some observations on the computational costs.

2.2.1. Traditional approximation methods

The first case considered uses traditional numerical methods, such as FEM [39], SEM [37], or FVM [26], to discretize the PDE system. These numerical approximations lead to large linear systems of equations that are extremely expensive computationally, rendering the solution of forward problems impractical in the context of sampling-based statistical techniques, such as MCMC. Yet, they provide well-defined theoretical error estimates, that typically depend on how fine the discretization (i.e., the tessellation of the computational domain via elements or grid points, also known as mesh) is. This property is particularly useful in the context of inverse problems, because it allows practitioners to have a clear understanding of the errors incurred within their solution framework.

In particular, when considering any of the numerical methods above, we can define a priori estimates on the error we might expect for a certain discretization level ℓ . The latter is usually defined in terms of mesh (or grid) size, h , that represents the dimensions of the elements (or spacing between grid points) tessellating the computational domain where the PDEs are being solved. For the purpose of this work, we assume an FEM-based discretization and the following generic error estimates.

Assumption 2.2. *Let u be the solution of the PDE equations in the forward problem. We assume that $u \in V$, where V is a suitable vector space, e.g. a Sobolev space. The FEM approximation error is given by*

$$\|u - u_\ell\|_V \leq C2^{-\ell}, \quad (7)$$

where ℓ is the level of discretization (each level ℓ halves the mesh size of the previous level $\ell - 1$) with the mesh size being defined as $h = 2^{-\ell}$.

Remark 2.1. *For simplicity, we did not include the error rate of time discretization. However, the time discretization error typically can be controlled by the discretization scheme to scale with the same rate of the spatial discretization. This will lead to the same convergence rate as in Assumption 2.2. Taking the finite-time two-dimensional Navier Stokes equation as an example, the error rate is $\|u(t) - u_\ell(t)\|_{H^1} \leq C\|h + \Delta t\|$ with a \mathbb{Q}_1 -iso- $\mathbb{Q}_2/\mathbb{Q}_1$ mixed Finite element discretization and Implicit/Explicit (IMEX) Euler time discretization scheme [18, 49].*

More details on error estimates for FEM can be found in [16, 20], while for SEM and FVM, the interested reader may refer to [30] and [38]. In analogy to Equation (4), we can define the numerical approximation of the forward map as follows

$$\mathcal{G}^\ell : U \rightarrow \mathbb{R}^k \quad \forall \mathbf{z} \in U; \quad \mathcal{G}^\ell(\mathbf{z}) = (\mathcal{F}_1(u_\ell(\mathbf{z})), \mathcal{F}_2(u_\ell(\mathbf{z})), \dots, \mathcal{F}_k(u_\ell(\mathbf{z}))). \quad (8)$$

where u_ℓ is the solution of the discrete forward problem and \mathcal{F}_i for $i = 1, \dots, k$ are k continuous bounded linear functionals. Thanks to Assumption 2.1, we can write the posterior probability measure also for the discrete problem we are considering here (in analogy with the continuous counterpart in Equation (5))

$$\frac{d\gamma^{\ell,y}}{d\gamma} \propto \exp(-\Phi^\ell(z; y)), \quad (9)$$

where $\Phi^\ell(z; y)$ is the discrete potential function. Given Assumption 2.2 and Equation (6), it follows immediately that the Hellinger distance metric between the continuous posterior γ^y and the discrete one $\gamma^{y,\ell}$ is bounded for every numerical refinement level ℓ

$$d_H(\gamma^y, \gamma^{y,\ell}) \leq C(y)2^{-\ell}, \quad (10)$$

where $C(y)$ is a positive constant, that depends only of the data y . Obviously, the larger the discretization level ℓ (i.e. the finer the mesh), the more computationally expensive the problem. In fact, the number of degrees of freedom of the corresponding discrete linear system increases exponentially with respect to ℓ . Hence, achieving a solution with a desired (and ideally small) error might be out of reach even with abundant computational resources. DL-based approximation methods (also referred to as DL-based surrogates) can come to the rescue here, and are introduced next.

2.2.2. DL-based approximation methods

The second case considered uses DL models to accelerate the solution of Bayesian inverse problems by replacing the computationally expensive numerical approximation just introduced in Section 2.2.1 with their fast inference properties. Let us denote $\tilde{\mathcal{G}} : U \rightarrow \mathbb{R}^k$ as a nonlinear map defined by a trained DL model. We assume that the DL model is trained with data generated with classical numerical methods, e.g. FEM, and that the objective is to solve the inverse problem with an error less than or equal to $\mathcal{O}(2^{-L})$. The procedure for solving such an inverse problem with DL-based surrogate acceleration is as follows.

First, we use a suitable numerical method (e.g. FEM, SEM, or FVM) to discretize the problem and generate the data. We assume that we use a characteristic mesh size equal to $h = \mathcal{O}(2^{-L})$; to achieve the target accuracy, thanks to Assumption 2.2. Second, we use the generated numerical data as training data for the DL model. Third, we use the trained DL model as a surrogate to quickly run an MCMC chain. The estimated expectation of the quantity of interest will be within the desired error if the DL-based surrogate model is as accurate as the numerical model.

However, empirically, the trained DL model can hardly achieve the same level of accuracy as the numerical approximation used to generate the training data, and will lead to additional error. We can formalize this statement as follows.

Assumption 2.3. *Given a DL model trained with data generated by a numerical approximation of the underlying forward problem that uses a mesh size $h = 2^{-L}$, and that has the error bound defined in Assumption 2.2, we can write*

$$\|\tilde{G}(\mathbf{z}) - u\|_V \leq 2^{-L+\epsilon}, \quad (11)$$

where \mathbf{z} is the input, and ϵ account for the error of the DL model. In order for the DL error to be a small, we require a small value of ϵ .

In practice, we expect ϵ to be small when we have a reasonably good DL model trained with sufficient data. However, in general, direct replacement of the numerical solver with a DL-based surrogate will lead to a posterior distribution estimation error of $\mathcal{O}(2^{-L+\epsilon})$ given by Equation (10). Hence, producing an error gap to the targeted $\mathcal{O}(2^{-L})$.

In order to mitigate the shortcomings of DL-based surrogate models, one can refine the mesh of the numerical model used for data generation and increase the size of the training data to produce a possibly more accurate DL model that can reach the desired accuracy. However, that will increase the computational cost by many folds. In general, to solve a two-dimensional problem, the minimum increment of the computational cost of the numerical model is 4 times, and 8 times for three-dimensional problems, not to mention more challenging problems whose computational cost does not scale linearly with the degree of freedoms. In addition to the cost of finer numerical solvers, the larger amount of data will also increase the DL training cost. Even if we are willing to pay the cost, it was shown that there is an empirical limit to the accuracy that certain DL models can reach [9]. Therefore, in some cases, the desired accuracy may be unreachable by direct substitution of the numerical model with a DL surrogate. In the next section, we propose a different approach to correct the error statistically with the MCMC method.

2.3. Hybrid two-level MCMC with uniform prior

In this section, we propose the hybrid two-level MCMC method for error correction of the DL-based surrogate model for Bayesian inverse problems. The new approach is inspired by the multilevel version of MCMC, which was shown to reduce the computational cost of standard MCMC for various problems by two orders of magnitude [15, 22, 24, 49]. Our hybrid two-level method utilizes both the DL-based surrogate model and the high-fidelity numerical model to sample the posterior probability of Bayesian inverse problems. In particular, we run a base MCMC chain with a DL-based surrogate, and a

correction MCMC chain with a numerical model with known accuracy. The latter is deployed to correct the statistical error of the MCMC chain generated by the DL-based surrogate.

Numerical multi-level approaches have been very successful for multi-scale physical problems. However, implementing multi-level algorithm for generic engineering or scientific problems can be challenging due to complex meshes and instability of coarse numerical models. We see the potential to avoid those challenges by hybridizing the DL-based surrogate and numerical solvers under the same mathematical framework. Hence, we propose a two-level hybrid approach inspired by the telescoping argument of the multilevel Monte Carlo algorithm [17]. We note that another potential approach is to use the DL-based surrogate model as a filter for the MCMC sampler, as inspired by [14]. However, we deem our proposed approach to be computationally more effective and more generalizable beyond the MCMC algorithm (i.e., our approach may also be applied to other filtering methods such as the ensemble Kalman filter and sequential Monte Carlo methods, among others).

We now start introducing our hybrid two-level MCMC method. To this end, we denote the quantity of interest as Q . This can be, for instance, the permeability field of the Darcy flow's subsurface model, or the initial condition of the Navier Stokes equations. We further indicate the posterior distribution approximated by the DL-based surrogate model as γ^{DL} , and the numerically approximated posterior distribution as γ^{num} . With the target precision of $\mathcal{O}(2^{-L})$ and Assumption 2.3, γ^{num} and γ^{DL} are equivalent to $\gamma^{L,y}$ and $\gamma^{L-\epsilon,y}$ in Section 2.2. In our two-level approach, we can rewrite the numerical approximation of the expected quantity of interest Q as follows

$$\begin{aligned}\mathbb{E}^{\gamma^{\text{num}}}[Q] &= \mathbb{E}^{\gamma^{\text{num}}}[Q] - \mathbb{E}^{\gamma^{\text{DL}}}[Q] + \mathbb{E}^{\gamma^{\text{DL}}}[Q] \\ &= \left(\mathbb{E}^{\gamma^{\text{num}}} - \mathbb{E}^{\gamma^{\text{DL}}}\right)[Q] + \mathbb{E}^{\gamma^{\text{DL}}}[Q].\end{aligned}\quad (12)$$

To derive a computable estimator with MCMC chains, we observe that the first term on the left hand side in (12) can be transformed as follows

$$\begin{aligned}\left(\mathbb{E}^{\gamma^{\text{num}}} - \mathbb{E}^{\gamma^{\text{DL}}}\right)[Q] &= \frac{1}{Z^{\text{num}}} \int_U \exp(-\Phi^{\text{num}}) Q d\gamma - \frac{1}{Z^{\text{DL}}} \int_U \exp(-\Phi^{\text{DL}}) Q d\gamma \\ &= \frac{1}{Z^{\text{num}}} \int_U \exp(-\Phi^{\text{num}}) (1 - \exp(\Phi^{\text{num}} - \Phi^{\text{DL}})) Q d\gamma \\ &\quad + \left(\frac{Z^{\text{DL}}}{Z^{\text{num}}} - 1\right) \frac{1}{Z^{\text{DL}}} \int_U \exp(-\Phi^{\text{DL}}) Q d\gamma,\end{aligned}\quad (13)$$

where the constant $(Z^{\text{DL}}/Z^{\text{num}} - 1)$ can be expanded as

$$\left(\frac{Z^{\text{DL}}}{Z^{\text{num}}} - 1\right) = \frac{1}{Z^{\text{num}}} \int_U (\exp(\Phi^{\text{num}} - \Phi^{\text{DL}}) - 1) \exp(-\Phi^{\text{num}}) d\gamma. \quad (14)$$

Having defined equations (12), (13), and (14), we can now define the hybrid two-level MCMC estimator $\mathbf{E}^{\text{hybrid}}[Q]$ of $\mathbb{E}^{\gamma^y}[Q]$ as

$$\begin{aligned} \mathbf{E}^{\text{hybrid}}[Q] &= \mathbf{E}_{M_{\text{num}}}^{\gamma^{\text{num}}} [(1 - \exp(\Phi^{\text{num}} - \Phi^{\text{DL}}))Q] \\ &\quad + \mathbf{E}_{M_{\text{num}}}^{\gamma^{\text{num}}} [\exp(\Phi^{\text{num}} - \Phi^{\text{DL}}) - 1] \cdot \mathbf{E}_{M_{\text{DL}}}^{\gamma^{\text{DL}}}[Q] + \mathbf{E}_{M_{\text{DL}}}^{\gamma^{\text{DL}}}[Q], \end{aligned} \quad (15)$$

where the M_{num} and M_{DL} is the number of numerical MCMC samples and DL surrogate MCMC samples. The new hybrid two-level MCMC approach for Bayesian inverse problems just introduced is simple, and it can therefore be adopted easily with legacy numerical models without too many changes in the code base. An important aspect of the new hybrid two-level MCMC introduced in equation (15) is its error analysis. In particular, we aim to show how the correction chain effectively corrects the estimator error caused by DL-based surrogate model. We decompose the error into three components:

$$\mathbb{E}^{\gamma^y}[Q] - \mathbf{E}^{\text{hybrid}}[Q] = \text{I} + \text{II} + \text{III}, \quad (16a)$$

$$\text{where } \text{I} := \mathbb{E}^{\gamma^y}[Q] - \mathbb{E}^{\gamma^{\text{num}}}[Q] \quad (16b)$$

$$\text{II} := \mathbb{E}^{\gamma^{\text{DL}}}[Q] - \mathbf{E}_{M_{\text{DL}}}^{\gamma^{\text{DL}}}[Q] \quad (16c)$$

$$\begin{aligned} \text{III} &:= \mathbb{E}^{\gamma^{\text{num}}} [(1 - \exp(\Phi^{\text{num}} - \Phi^{\text{DL}}))Q] \\ &\quad - \mathbf{E}_{M_{\text{num}}}^{\gamma^{\text{num}}} [(1 - \exp(\Phi^{\text{num}} - \Phi^{\text{DL}}))Q] \\ &\quad + \mathbb{E}^{\gamma^{\text{num}}} [\exp(\Phi^{\text{num}} - \Phi^{\text{DL}}) - 1] \cdot \mathbb{E}^{\gamma^{\text{DL}}}[Q] \\ &\quad - \mathbf{E}_{M_{\text{num}}}^{\gamma^{\text{num}}} [\exp(\Phi^{\text{num}} - \Phi^{\text{DL}}) - 1] \cdot \mathbf{E}_{M_{\text{DL}}}^{\gamma^{\text{DL}}}[Q] \end{aligned} \quad (16d)$$

Proof. Given the estimator error, we observe

$$\begin{aligned} \mathbb{E}^{\gamma^y}[Q] - \mathbf{E}^{\text{hybrid}}[Q] &= \mathbb{E}^{\gamma^y}[Q] - \mathbb{E}^{\gamma^{\text{num}}}[Q] + \mathbb{E}^{\gamma^{\text{num}}}[Q] - \mathbf{E}^{\text{hybrid}}[Q] \\ &= \text{I} + \mathbb{E}^{\gamma^{\text{num}}}[Q] - \mathbf{E}^{\text{hybrid}}[Q] \end{aligned} \quad (17)$$

With equation (13) and (15), we have

$$\begin{aligned}
\mathbb{E}^{\gamma^y}[Q] - \mathbf{E}^{\text{hybrid}}[Q] &= \text{I} + \mathbb{E}^{\gamma^{\text{num}}}[Q] - \mathbf{E}^{\text{hybrid}}[Q] \\
&= \text{I} + \mathbb{E}^{\gamma^{\text{DL}}}[Q] + \mathbb{E}^{\gamma^{\text{num}}}[(1 - \exp(\Phi^{\text{num}} - \Phi^{\text{DL}}))Q] \\
&\quad + \mathbb{E}^{\gamma^{\text{num}}}[\exp(\Phi^{\text{num}} - \Phi^{\text{DL}}) - 1] \cdot \mathbb{E}^{\gamma^{\text{DL}}}[Q] - \mathbf{E}_{M_{\text{DL}}}^{\gamma^{\text{DL}}}[Q] \\
&\quad - \mathbf{E}_{M_{\text{num}}}^{\gamma^{\text{num}}}[(1 - \exp(\Phi^{\text{num}} - \Phi^{\text{DL}}))Q] \\
&\quad - \mathbf{E}_{M_{\text{num}}}^{\gamma^{\text{num}}}[\exp(\Phi^{\text{num}} - \Phi^{\text{DL}}) - 1] \cdot \mathbf{E}_{M_{\text{DL}}}^{\gamma^{\text{DL}}}[Q] \\
&= \text{I} + \text{II} + \text{III}. \tag{18}
\end{aligned}$$

□

As shown, the overall error bound for our hybrid two-level MCMC method is composed of three error terms in equation (16). We analyse each error term individually, and assemble the overall error result as a conclusion to this analysis.

For error term I, from equation (16) and equation (10), we can obtain the following error bound

$$\text{I} := \mathbb{E}^{\gamma^y}[Q] - \mathbb{E}^{\gamma^{\text{num}}}[Q] \leq C2^{-L}. \tag{19}$$

For error term II, from Proposition 5 in [24] we can obtain the following error bound

$$\text{II} := \mathbb{E}^{\gamma^{\text{DL}}}[Q] - \mathbf{E}_{M_{\text{DL}}}^{\gamma^{\text{DL}}}[Q] \leq M_{\text{DL}}^{-1/2}, \tag{20}$$

which is a standard result from Markov chain theory.

Finally, for error term III, we can use the inequality $|\exp(x) - \exp(y)| \leq |x - y|(\exp(x) + \exp(y))$, to obtain

$$\begin{aligned}
\sup_{z \in U} |1 - \exp(\Phi^{\text{num}} - \Phi^{\text{DL}})| &\leq \sup_{z \in U} |\Phi^{\text{num}} - \Phi^{\text{DL}}| (1 + \exp(\Phi^{\text{num}} - \Phi^{\text{DL}})) \\
&\leq C(1 + 2^\epsilon)2^{-L}, \tag{21}
\end{aligned}$$

that leads to

$$\begin{aligned}
&\mathbf{E}[\{\mathbb{E}^{\gamma^{\text{num}}}[(1 - \exp(\Phi^{\text{num}} - \Phi^{\text{DL}}))Q] \\
&\quad - \mathbf{E}_{M_{\text{num}}}^{\gamma^{\text{num}}}[(1 - \exp(\Phi^{\text{num}} - \Phi^{\text{DL}}))Q]\}^2] \leq CM_{\text{num}}^{-1}(1 + 2^\epsilon)^2 2^{-2L}. \tag{22}
\end{aligned}$$

Similarly, we have

$$\begin{aligned}
& \mathbf{E}[\{\mathbb{E}^{\gamma^{\text{num}}}[\exp(\Phi^{\text{num}} - \Phi^{\text{DL}}) - 1] \cdot \mathbb{E}^{\gamma^{\text{DL}}}[Q] \\
& \quad - \mathbf{E}_{M_{\text{num}}}^{\gamma^{\text{num}}}[\exp(\Phi^{\text{num}} - \Phi^{\text{DL}}) - 1] \cdot \mathbf{E}_{M_{\text{DL}}}^{\gamma^{\text{DL}}}[Q]\}^2] \\
& \leq C\mathbf{E}[\{\mathbb{E}^{\gamma^{\text{num}}}[\exp(\Phi^{\text{num}} - \Phi^{\text{DL}}) - 1] \\
& \quad - \mathbf{E}_{M_{\text{num}}}^{\gamma^{\text{num}}}[\exp(\Phi^{\text{num}} - \Phi^{\text{DL}}) - 1]\}^2] \cdot \sup_{z \in U} |Q|^2 \\
& \quad + C \sup_{z \in U} |\exp(\Phi^{\text{num}} - \Phi^{\text{DL}}) - 1|^2 \cdot \mathbf{E}[\{\mathbb{E}^{\gamma^{\text{DL}}}[Q] - \mathbf{E}_{M_{\text{DL}}}^{\gamma^{\text{DL}}}[Q]\}^2] \\
& \leq CM_{\text{num}}^{-1}(1 + 2^\epsilon)^2 2^{-2L} + CM_{\text{DL}}^{-1}(1 + 2^\epsilon)^2 2^{-2L}. \tag{23}
\end{aligned}$$

By combining equations (22) and (23), we have the overall error estimate for III, that is

$$\begin{aligned}
\text{III} & := \mathbb{E}^{\gamma^{\text{num}}}[(1 - \exp(\Phi^{\text{num}} - \Phi^{\text{DL}}))Q] \\
& \quad - \mathbf{E}_{M_{\text{num}}}^{\gamma^{\text{num}}}[(1 - \exp(\Phi^{\text{num}} - \Phi^{\text{DL}}))Q] \\
& \quad + \mathbb{E}^{\gamma^{\text{num}}}[\exp(\Phi^{\text{num}} - \Phi^{\text{DL}}) - 1] \cdot \mathbb{E}^{\gamma^{\text{DL}}}[Q] \\
& \quad - \mathbf{E}_{M_{\text{num}}}^{\gamma^{\text{num}}}[\exp(\Phi^{\text{num}} - \Phi^{\text{DL}}) - 1] \cdot \mathbf{E}_{M_{\text{DL}}}^{\gamma^{\text{DL}}}[Q] \\
& \leq CM_{\text{num}}^{-1}(1 + 2^\epsilon)^2 2^{-2L} + CM_{\text{DL}}^{-1}(1 + 2^\epsilon)^2 2^{-2L}.
\end{aligned}$$

Until now, we are still free to choose the number of samples for M_{num} and M_{DL} . To balance the error I, II and III, we can choose the sampling number $M_{\text{DL}} = C2^{2L}$ and $M_{\text{num}} = C(1 + 2^\epsilon)^2$, that allows us to write overall error estimate.

Theorem 2.1. *With $M_{\text{DL}} = C2^{2L}$ and $M_{\text{num}} = C(1 + 2^\epsilon)^2$, we have the following theoretical error estimate of our hybrid two-level MCMC approach under uniform priors*

$$\mathbf{E}[|\mathbb{E}^{\gamma^y}[Q] - \mathbf{E}^{\text{hybrid}}[Q]|] \leq C2^{-L}. \tag{24}$$

Theorem 2.1 gives the estimation error of the hybrid two-level MCMC algorithm with the chosen number of samples for each chain. We can observe that the estimation error is as good as the one from a plain MCMC algorithm with only numerical samples. In addition, if we assume the speedup rate of the DL-based surrogate model as s , we can estimate the overall speedup of

our new hybrid two-level approach compared to the plain numerical MCMC. In particular, with the choice of samples M_{DL} and M_{num} , the overall speedup is $\mathcal{O}(2^{2L} / (\frac{1}{s}2^{2L} + (1+2^\epsilon)^2))$ compared to the plain numerical MCMC. We note that the hybrid two-level approach can be easily parallelized with two processes, thus the actual speedup is $\mathcal{O}(2^{2L} / \max(\frac{1}{s}2^{2L}, (1+2^\epsilon)^2))$. Even though the discussion is based on the setup of a uniform prior, the same conclusions hold for Gaussian priors. Details of the latter are provided in Appendix A. In Section 3, we show several experiments that validate the theoretical findings.

As a final note, we shall point out that, even though the hybrid method is able to provide accurate posterior expectations of the quantities of interest and the variance (which can be computed from the expectations), the method will not generate a large number of actual numerical samples from the highly accurate numerically approximated posterior distribution (the exact reason why computational cost is saved). This limits the method from producing a histogram like a conventional MCMC chain. However, a less accurate histogram can still be generated from the DL surrogate samples.

3. Numerical experiments

After having introduced the new hybrid two-level MCMC approach, we now present some numerical experiments to validate the theoretical error estimates and to understand the computational performance of the new approach. The numerical experiments span three different PDE problems, namely the Poisson equation, the reaction-diffusion equation, and the Navier-Stokes equations. These three problems include both elliptic and parabolic differential problems, with different levels of complexity, and constitute an established benchmark for testing novel methods in the context of Bayesian inverse problems [47].

In the numerical experiments, we consider both uniform and Gaussian priors, to demonstrate the theoretical error estimates presented in Sections 2.3, and Appendix A, respectively.

All results are obtained in two-dimensional squared computational domains (or meshes) $\Omega_h \in [0, 1] \times [0, 1]$, Mesh A, and Mesh B, depicted in Figure 2, where we observe the solution u in equally spaced fixed positions, highlighted as red crosses. Mesh A in Figure 2a is used for the numerical experiments with the Poisson equation and the reaction-diffusion equation, and has a number of cells equal to $32 \times 32 = 1024$. Mesh B in Figure 2b is

used for the numerical experiment with the Navier-Stokes equation, and has a number of cells $64 \times 64 = 4096$.

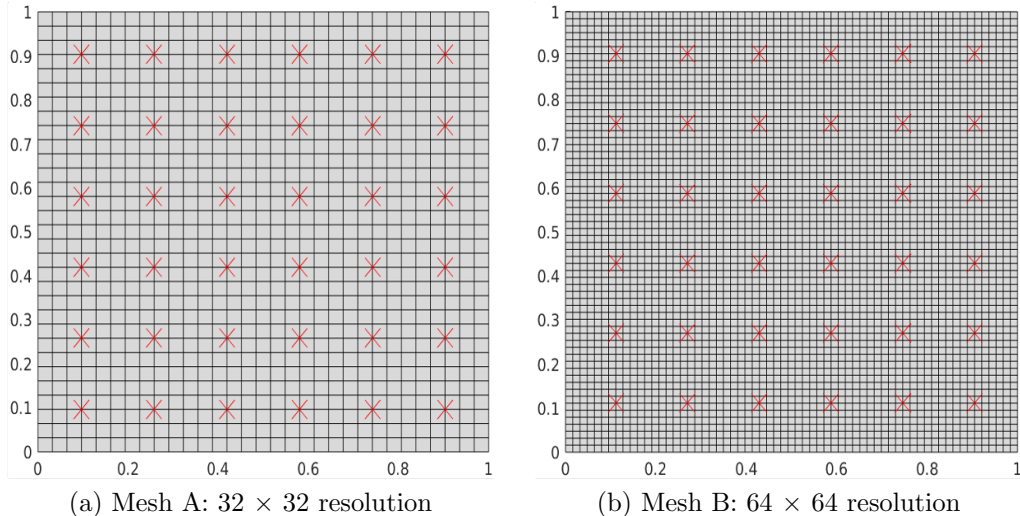


Figure 2: Meshes adopted and points where the solution is observed (red crosses). Mesh A is used for the numerical experiments on the Poisson and reaction-diffusion equations, while Mesh B is used for the numerical experiments on the Navier-Stokes equations.

For the different problems considered, we used a range of different neural network architectures, to show that the method proposed here is agnostic to the choice of DL surrogate. The list of experiments carried out in the following subsections is summarized in Table 1.

	1	2	3	4	5	6
Problem	Poisson Equation	Reaction Diffusion	Navier Stokes			
Prior	Uniform	Gaussian	Uniform	Gaussian	Uniform	Gaussian
DL Model	FCN	CNN	GNN	U-Net	DeepONet	FNO
Section	3.1.1	3.1.2	3.2.1	3.2.1	3.3.1	3.3.1

Table 1: List of numerical experiments

3.1. Poisson equation

We first consider the Bayesian inverse problem with the forward model governed by the Poisson equation in the two-dimensional computational do-

main depicted in Figure 2a.

$$\begin{cases} \nabla \cdot (K \nabla u(x)) = \cos(2\pi x_1) \sin(2\pi x_2), \\ u(x_1 = 0) = 0, \\ u(x_1 = 1) = 1, \\ \frac{\partial u}{\partial x_2}(x_2 = 0) = \frac{\partial u}{\partial x_2}(x_2 = 1) = 0. \end{cases} \quad (25)$$

The data u is observed at thirty-six equally-distanced positions, as shown in figure 2a, using a random realization of the forward model with additive Gaussian noise δ that has zero mean and variance $\sigma^2 = 0.001$. We next present the uniform and Gaussian prior cases.

3.1.1. Uniform prior

For this first case, we set the quantity of interest to be the random field $K = z \cos(2\pi x_1) \sin(2\pi x_2) + 2.0$, whereby its prior distribution is uniform, namely $z \sim U[-1, 1]$. We solve equation (25) using FEM on Mesh A (depicted in Figure 2a), and randomly generate 8000 solution samples. The 8000 samples are partitioned into 4000 training samples, 2000 validation samples, and 2000 test samples to train a fully connected ReLU neural network. For details on the FEM solver and the neural network model, the interested reader may refer to Appendix B.1. We experimentally estimate the mean surrogate model error and numerical model error by Gaussian Legendre quadrature method to obtain an estimation of the ϵ value mentioned in Assumption 2.3. The quadrature methods samples 32 samples of z from $U[-1, 1]$ to estimate the mean error in comparison to reference solutions. Reference solutions are obtained on an extremely fine mesh (compared to Mesh A) and composed of $1024 \times 1024 = 1048576$ elements.

We have the following estimator of the expected L^2 surrogate error $\mathbf{E}(|u_{L=10} - u_{L=5}|_{L^2}) = 5.576e^{-5}$ and $\mathbf{E}(|u_{L=10} - u_{DL}|_{L^2}) = 3.132e^{-4}$. With such, we have a rough estimate of $\epsilon = 2.49$. With reference to Theorem 2.1, the correction chain only needs around 4% numerical samples compared to the long DL-based MCMC chain (which also means we need only 4% numerical samples compared to a standard numerical MCMC targeting the same error rate).

We performed numerical experiments on three setups: (i) a plain MCMC chain with numerical solver, denoted as **Numerical MCMC** in Table 2, (ii) a plain MCMC chain with DL-based surrogate model, denoted as **DL**

MCMC in Table 2, (iii) and the proposed hybrid approach, denoted as **Hybrid MCMC** in Table 2, where we considered two cases (given the theoretical estimates just introduced), one with 4% numerical samples and the other with 40% numerical samples (compared to the total number of samples).

The average results of five MCMC runs are shown in Table 2. The reference value computed via FEM with 32 Gaussian Legendre quadrature points is also included. Quadrature estimation of the posterior mean are included in Table 2 for numerical models with discretization level $l = 10$ and $l = 5$, each with mesh size 2^{-10} and 2^{-5} , denoted as **Quad L=10**, **Quad L=5**. **Quad L=10** provides a highly accurate posterior expectation which can be considered as a true reference. Hence, all the estimator errors are calculated by comparing to **Quad L=10**. We observe how the proposed hybrid two-level MCMC approach provides results that are comparable to the numerical MCMC method. The comparison between the two hybrid MCMC experiments also validates Theorem 2.1, where our estimate is close to optimal and additional numerical samples do not further improve the results.

Finally, we estimated the overall computational time of the hybrid two-level MCMC approach compared to the numerical MCMC and DL MCMC. The estimation is based on the average runtime for one numerical sample and one DL-based surrogate sample. The FEM solver uses Intel Xeon E5-2620 CPU, while the DL-based surrogate model inferences used one NVIDIA RTX A6000 GPU (we use the same CPU and GPU specs for all the subsequent experiments). Thanks to the fact that the two MCMC chains in the hybrid MCMC method can be run concurrently, the hybrid MCMC with 100,000 surrogate samples and 4,000 numerical samples achieved the same speed up as the plain MCMC with purely surrogate samples, but achieving a smaller error.

Method	Quad L=10	Quad L=5	Numerical MCMC	DL MCMC	Hybrid MCMC	Hybrid MCMC
Samples	-	-	100,000	100,000	100,000 +4,000	100,000 +40,000
Quantity of interest	0.313237	0.312763	0.312265	0.305713	0.313032	0.312943
Estimator error	-	0.000474	0.000972	0.007524	0.000205	0.000294
Compute time [s]	-	-	1090.95	65.77	65.77	435.79
Speed up	-	-	-	16.59x	16.59x	2.50x

Table 2: Expectation of quantity of interest for the elliptic problem with uniform prior

3.1.2. Gaussian (log-normal) prior

In contrast to the uniform prior case just shown, for this experiment, the quantity of interest K is spatially varying, that is: $K = K(x)$, and we assume its prior distribution to be sampled from the following bi-Laplacian Gaussian prior

$$\mathcal{A}m = \begin{cases} \gamma \nabla \cdot (\Xi \nabla m) + \delta m & \text{in } \Omega \\ (\Xi \nabla m) \cdot \mathbf{n} + \beta m & \text{on } \partial\Omega, \end{cases} \quad (26)$$

where $\gamma = 0.1$, $\delta = 0.5$, $\beta = \sqrt{\gamma\delta}$ and Ξ controls the anisotropy where we use an identity matrix. In the numerical experiments, the covariance matrix \mathcal{A}^{-2} is obtained by discretizing Equation (26) to get the non-negative random field sample $K(x) = \exp(m)$ from the random field sample m generated via the bi-Laplacian prior. We show four examples of random samples generated in this experiment in Figure 3.

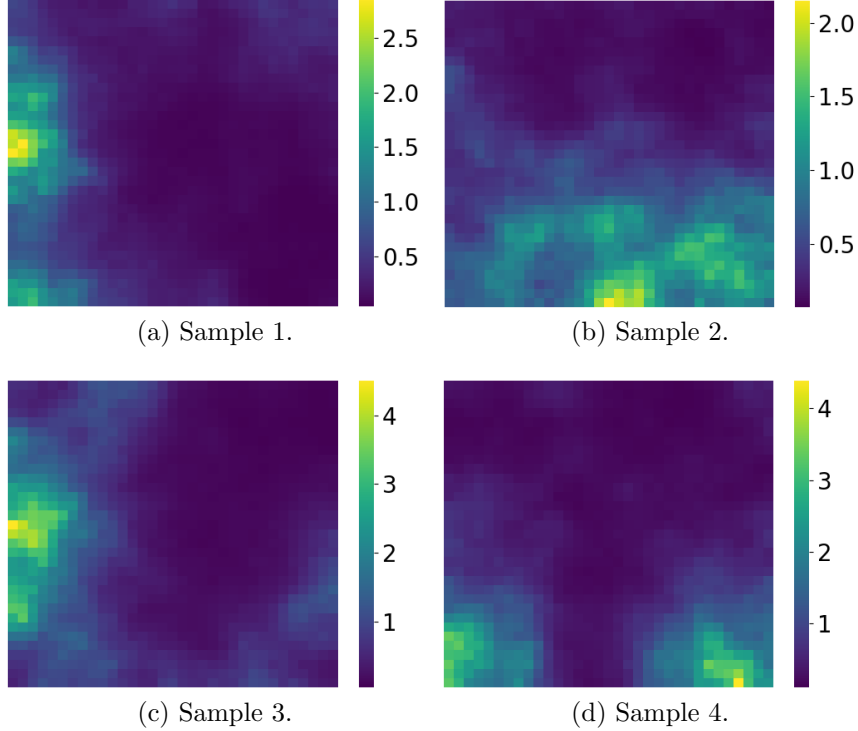


Figure 3: Samples obtained from the bi-Laplacian random field in equation (26) for the Poisson equation with Gaussian prior.

Similarly to the uniform-prior case, we solve the forward problem in equation (25) via FEM on Mesh A (Figure 2a), and generate 8000 random samples. Again, the 8000 samples are partitioned into 4000 training samples, 2000 validation samples, and 2000 test samples to train a convolutional neural network. The convolutional neural network consists of 3 encoding layer, 1 fully connected layers and 3 decoding layers, and it is trained using the Adam optimized for 10000 epochs. In analogy with the uniform-prior case, we run three experiments: (i) a plain MCMC chain with numerical solver, denoted as **Numerical MCMC** in Table 3, (ii) a plain MCMC chain with DL-based surrogate model, denoted as **DL MCMC** in Table 3, and the proposed hybrid approach, denoted as **Hybrid MCMC** in Table 3, where we considered three cases, 1%, 5%, and 10% numerical samples (compared to the total number of samples).

The average results of five MCMC runs are depicted in Figure 4. The expectation of the posterior from the MCMC chains generated solely with a

DL-based surrogate model has obvious discrepancies with the plain MCMC chains generated solely with a numerical solver (that constitute the reference). Our hybrid two-level MCMC approach, with the addition of only few numerical samples, is able to significantly improve the results making it comparable to the reference, at a fraction of the computational cost.

We summarize the results in Table 3, where the L^2 and L^∞ difference between the DL-based surrogate accelerated MCMC results and classical numerical MCMC results are presented. From the results presented, there are significant improvements in terms of accuracy with the hybrid approach. With only 1% additional numerical samples on top of the DL-based MCMC chain, the results get much closer to the one from the numerical MCMC. With 4% or more additional numerical samples, the hybrid approach is on par with the plain numerical MCMC, while being significantly cheaper computationally.

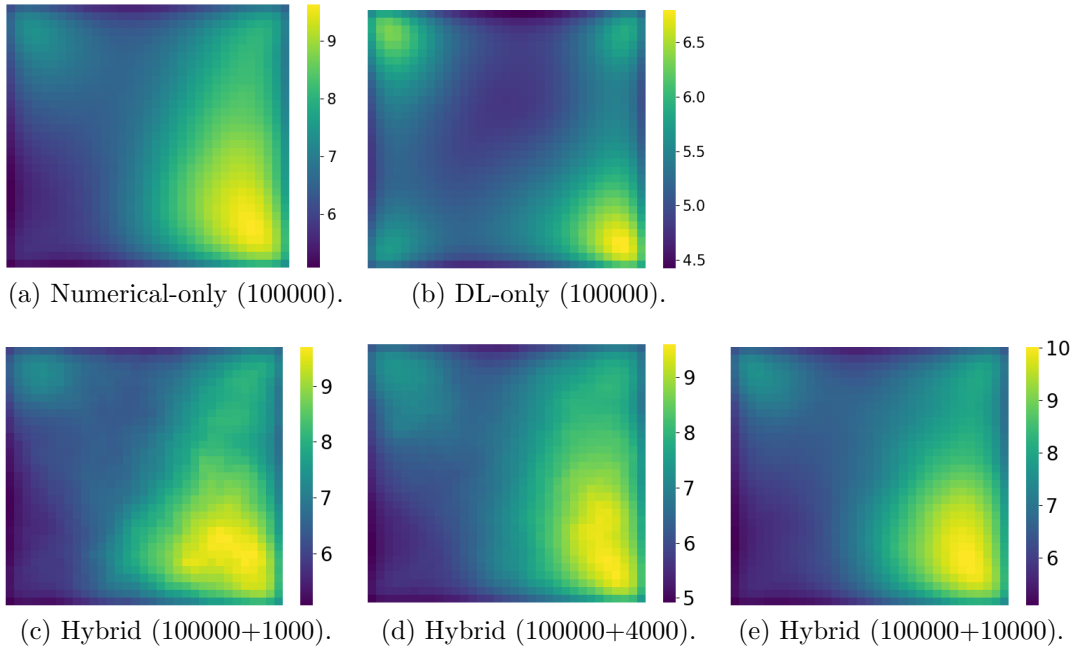


Figure 4: Expected mean of $K(x)$ from 5 runs of MCMC with elliptic equation with Gaussian prior.

Method	Numerical MCMC	DL MCMC	Hybrid MCMC	Hybrid MCMC	Hybrid MCMC
Samples	100,000	100,000	100,000 + 1,000	100,000 + 4,000	100,000 + 10,000
L^2 difference from numerical MCMC	-	0.009374	0.002471	0.000492	0.000452
L^∞ difference from numerical MCMC	-	0.483396	0.177329	0.047232	0.036976
Compute time [s]	1080.67	70.54	70.54	70.54	108.54
Speed up	-	15.32x	15.32x	15.32x	10x

Table 3: Difference between the posterior expectation results of plain numerical MCMC and the posterior expectation results of the plain and hybrid DL-based MCMC with elliptic equation with Gaussian prior

3.2. Reaction-diffusion equation

We consider the Bayesian inverse problem with the forward model governed by the following reaction-diffusion equation in a two-dimensional unit square domain Ω

$$\begin{cases} \nabla \cdot (K(x)\nabla u(x)) + u^3 = 0, \\ u(x_1 = 0) = 0, \\ u(x_1 = 1) = 1, \\ \frac{\partial u}{\partial x_2}(x_2 = 0) = \frac{\partial u}{\partial x_2}(x_2 = 1) = 0. \end{cases} \quad (27)$$

Thirty-six equally distanced observations are captured from a random realization of the forward model with additional Gaussian noise δ with zero mean and variance $\sigma^2 = 0.1$.

3.2.1. Uniform prior

In this section, we consider the uniform prior case with a random field $K(x)$ that depends on uniformly distributed coefficients $z_i, i = 0, 1, \dots, 4$

$$\begin{aligned} \ln(K(x)) = & z_0 + z_1 \cos(2\pi x_1) \sin(2\pi x_2) + z_2 \sin(2\pi x_1) \cos(2\pi x_2) \\ & + z_3 \cos(2\pi x_1) \cos(2\pi x_2) + z_4 \sin(2\pi x_1) \sin(2\pi x_2), \end{aligned}$$

where $z_i \sim U[-1, 1], i = 0, 1, \dots, 4$. We solve the reaction diffusion equation (27) with the FEM method on a 36×36 uniformly spaced Mesh A 2a. We randomly generated 4000 samples with a FEM numerical solver. The 4000 data are partitioned into 2000 training samples, 1000 validation samples, and 1000 test samples. We train a vanilla Message Passing Graph Neural Network (MPGNN) as our DL surrogate. The details of the FEM solver and the Graph Neural Network architecture can be found in Section Appendix B.2. We run three experiments: (i) a plain MCMC chain with numerical solver, denoted as **Numerical MCMC** in Table 4, (ii) a plain MCMC chain with the MPGNN-based DL surrogate model, denoted as **DL MCMC** in Table 4, and the proposed hybrid approach, denoted as **Hybrid MCMC** in Table 4, where we considered three cases, 1%, 5%, and 10% numerical samples (compared to the total number of samples).

The average results of five MCMC runs are presented in Figure 5. The L^2 and L^∞ difference between the numerical MCMC results and the DL-based methods (including the DL MCMC and the Hybrid MCMC) are presented in Table 4. These show that the additional numerical samples in the hybrid method reduce both L^2 and L^∞ difference compared to the DL MCMC method. The results validate the theoretical conclusion in Theorem 2.1, that the hybrid two-level approach can reach the same accuracy level as the numerical MCMC at an additional small fraction of the computational cost. Due to the fact that two MCMC chains can run in parallel in this particular experiment, the actual time taken by the hybrid approach with 5% numerical samples is the same as the run time of the DL MCMC. However, the hybrid approach provides a more accurate result.

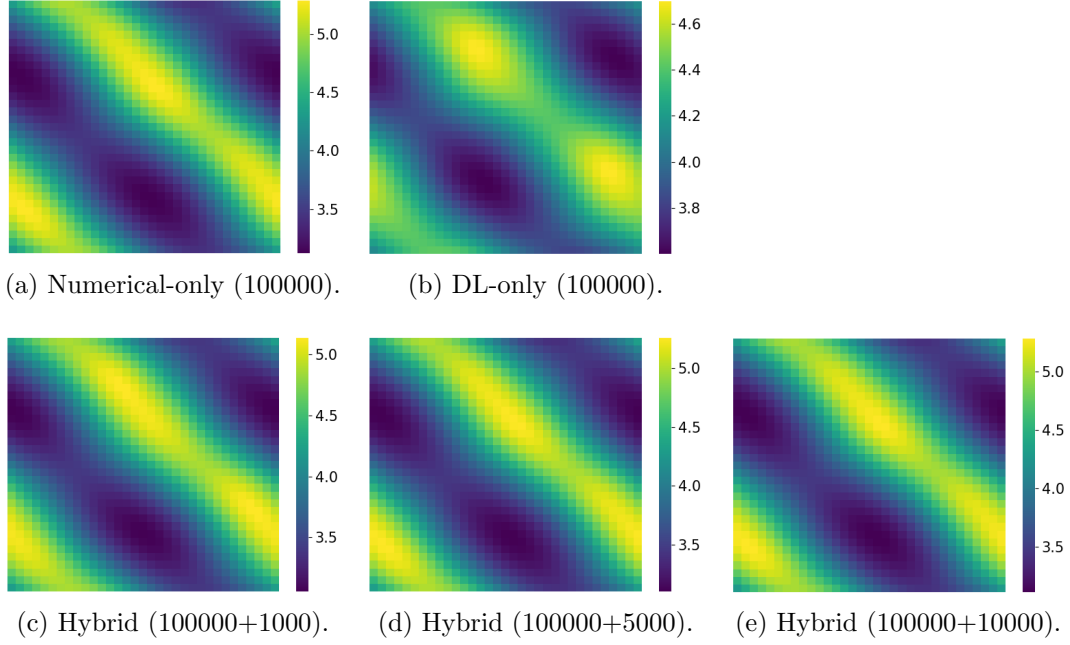


Figure 5: Expected mean of $K(x)$ from 5 runs of MCMC with reaction diffusion equation with uniform prior.

Method	Numerical MCMC	DL MCMC	Hybrid MCMC	Hybrid MCMC	Hybrid MCMC
Samples	100,000	100,000	100,000 + 1,000	100,000 + 5,000	100,000 + 10,000
L^2 difference from numerical MCMC	-	0.002914	0.000702	0.000188	0.000137
L^∞ difference from numerical MCMC	-	0.177232	0.044160	0.012106	0.009616
Compute time [s]	2840.75	65.78	65.78	65.78	284.08
Speed up	-	43.19x	43.19x	43.19x	10x

Table 4: Difference between the posterior expectation results of plain numerical MCMC and the posterior expectation results of the plain and hybrid DL-based MCMC with non-linear reaction-diffusion equation with uniform prior

3.2.2. Gaussian prior

We consider the $K(x)$ to be of Gaussian random distribution. We sample the Gaussian random field again from the following bi-Laplacian Gaussian prior.

$$\mathcal{A}m = \begin{cases} \gamma \nabla \cdot (\Xi \nabla m) + \delta m & \text{in } \Omega \\ (\Xi \nabla m) \cdot \mathbf{n} + \beta m & \text{on } \partial\Omega \end{cases}$$

where we have $\gamma = 0.1$, $\delta = 0.5$, $\beta = \sqrt{\gamma\delta}$ and Ξ an identity matrix. In the numerical experiment, a non-negative random field is generated as $K(x) = \exp(m)$ with m a random field sample generated from the bi-Laplacian prior. We solve the above equation with the Finite Element Method with uniformly spaced mesh with a 32×32 mesh resolution. We randomly generated 4000 samples with the Finite Element solver. The 4000 data are partitioned into 2000 training data, 1000 validation data, and 1000 test data to train a U-net neural network. The details of the FEM solver and the neural network architecture can be found in Section Appendix B.2.

We performed numerical experiments on three setups: (i) a plain MCMC chain with numerical solver, denoted as **Numerical MCMC** in Table 5, (ii) a plain MCMC chain with DL-based surrogate model, denoted as **DL MCMC** in Table 5, (iii) and the proposed hybrid approach, denoted as **Hybrid MCMC** in Table 5, where we considered three cases, 1%, 5%, and 10% numerical samples (compared to the total number of samples).

The results of the average of the five MCMC run are shown in Figure 6. The L^2 and L^∞ difference between MCMC results generated with the DL-based surrogate and plain numerical MCMC are included in Table 5. The results show that the additional numerical samples in the hybrid method reduce both L^2 and L^∞ difference compared to the plain MCMC model.

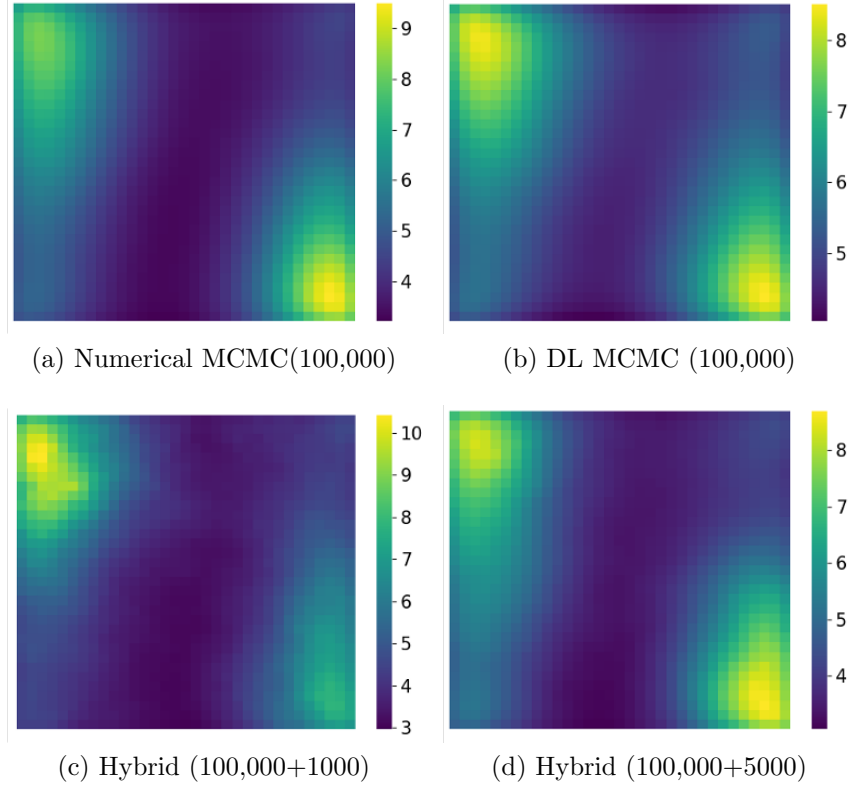


Figure 6: Expected mean of $K(x)$ from 5 runs of MCMC using the reaction-diffusion equation

Method	Numerical MCMC	DL MCMC	Hybrid MCMC	Hybrid MCMC	Hybrid MCMC
Samples	100,000	100,000	100,000 + 1,000	100,000 + 5,000	100,000 + 10,000
L^2 difference from numerical MCMC	-	0.005811	0.002908	0.001055	0.000605
L^∞ difference from numerical MCMC	-	0.303029	0.268921	0.096580	0.063807
Compute time [s]	3396.72	178.81	178.81	178.81	339.67
Speed up	-	18.99x	18.99x	18.99x	10x

Table 5: Difference between the posterior expectation results of plain numerical MCMC and the posterior expectation results of the plain and hybrid DL-based MCMC with non-linear reaction-diffusion equation with Gaussian prior

3.3. avier Stokes equations

We consider the Bayesian inverse problem with the forward model governed by the two dimensional Navier Stokes equations in the vorticity form in a domain of two-dimensional unit torus \mathbb{T}^2 ,

$$\begin{cases} \frac{\partial \omega(x, t)}{\partial t} + u(x, t) \cdot \nabla \omega(x, t) - \nu \Delta \omega(x, t) = f, & \text{for } x \in \mathbb{T}^2, \\ \nabla \cdot u(x, t) = 0, & \text{for } x \in \mathbb{T}^2, \\ \omega(x, 0) = \omega_0; \end{cases} \quad (28)$$

with periodic boundary conditions and the random forcing

$$f = 0.1(\sin(2\pi(x_1 + x_2)) + \cos(2\pi(x_1 + x_2))). \quad (29)$$

ω is the vorticity, u is the velocity, and $\nu = 0.001$ is the viscosity. Thirty-six equally distanced observations are captured from a random realization of the forward model with additional Gaussian noise δ with zero mean and variance $\sigma^2 = 1$.

3.3.1. Uniform prior

In this section, we consider the uniform prior case, using a Fourier expansion of ω_0 with coefficient of each Fourier term uniformly distributed

$$Z_{ij} = z_{ij} N^2 \sqrt{2} \cdot 7^{3/2} (4\pi^2(k_i^2 + k_j^2) + 49)^{-5/4},$$

where $N = 64$ is the number of modes in each axis, k_i and k_j are the mode index in the x and y directions, and $z_{ij} \sim U[-1, 1]$. Using the inverse fast Fourier transform (ifft), we have

$$\omega_0 = \text{ifft}(Z).$$

We solve the two-dimensional Navier-Stokes equations (28) by using a pseudospectral method with Crank-Nicolson time integration on Mesh B, that is composed of 64×64 collocation points. We randomly generated 8000 samples with the numerical solver, where 4000 samples are used for training, 2000 for validation, and 2000 for testing. DeepONet is used as the DL-based surrogate model. For more details on the numerical solver and the DL architecture, the interested reader can refer to Section Appendix B.3.

We run three experiments: (i) a plain MCMC chain with numerical solver, denoted as **Numerical MCMC** in Table 6, (ii) a plain MCMC chain with DL-based surrogate model, denoted as **DL MCMC** in Table 6, and the proposed hybrid approach, denoted as **Hybrid MCMC** in Table 6, where we considered two cases, 5%, and 10% numerical samples (compared to the total number of samples). The average results of eight MCMC runs are presented in Figure 7. The quantitative numerical comparison of the posterior expectation is included in Table 6. Despite the small DL surrogate error of the trained DeepONet model shown in the experiment, we still see improvement in terms of L^2 and L^∞ difference compared to the posterior expectation of the numerical MCMC. We note that in this case the DL MCMC based on DeepONet already achieves relatively good performance, and it is the obviously the fastest method. Marginal accuracy gains are achieved by using our hybrid approach. Indeed, this is not surprising, as the theoretical estimated proposed in Section 2.3 indicate that the DL MCMC has already an error close to the theoretical estimates. Hence, adding some numerical samples within our hybrid MCMC does not significantly improves the results. This demonstrates that the theoretical framework developed can be used to understand whether a DL MCMC can be used for a given Bayesian inverse problem, or some numerical samples may be required instead.

Method	Numerical MCMC	DL MCMC	Hybrid MCMC	Hybrid MCMC
Samples	100,000	100,000	100,000 + 5,000	100,000 + 10,000
L^2 difference from numerical MCMC	-	9.01488e-05	4.65333e-05	3.88844e-05
L^∞ difference from numerical MCMC	-	0.015763	0.011152	0.008156
Compute time [s]	794901.33	846.78	39745.07	79490.13
Speed up	-	938.73x	20x	10x

Table 6: Difference between the posterior expectation results of plain numerical MCMC and the posterior expectation results of the plain and hybrid DL-based MCMC with Navier Stokes equations with uniform prior

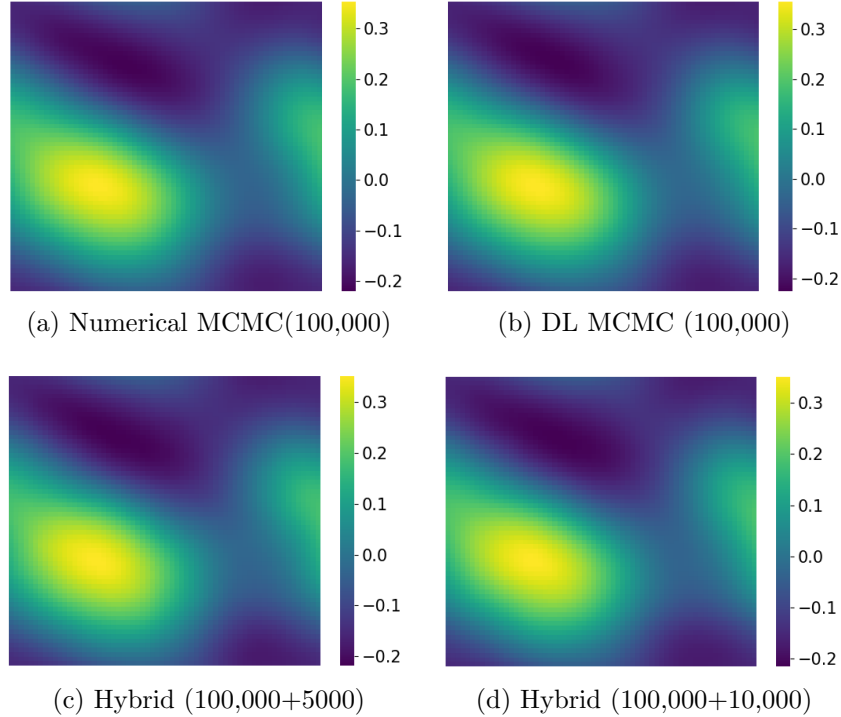


Figure 7: Expected mean of $K(x)$ from 5 runs of MCMC using the Navier Stokes Equations with uniform prior

3.3.2. Gaussian prior

In this section, we consider the Gaussian prior case, focusing on ω_0 . We sample the Gaussian random field from the following bi-Laplacian Gaussian prior with the following distribution: $\mathcal{N}(0, 7^{\frac{3}{2}}(-\Delta + 49I)^{-2.5})$. We solve the above equation with the pseudo-spectral method with the Crank-Nicolson time integration method. In this experiment a resolution of 64×64 is used. We randomly generated 4000 samples with the numerical solver. The 4000 data are partitioned into 2000 training data, 1000 validation data, and 1000 test data to train the Fourier Neural Operator (FNO) as described in [33]. Details of the DL-based surrogate model setup can be found in Appendix B.3.

We run three experiments: (i) a plain MCMC chain with numerical solver, denoted as **Numerical MCMC** in Table 7, (ii) a plain MCMC chain with DL-based surrogate model, denoted as **DL MCMC** in Table 7, and the

proposed hybrid approach, denoted as **Hybrid MCMC** in Table 7, where we considered three cases, 1%, 5%, and 10% numerical samples (compared to the total number of samples).

The results of the average of the eight MCMC run are concluded in Figure 8. We can see the posterior mean of the three methods, plain numerical MCMC, plain MCMC by DL-based surrogate model, and hybrid MCMC. The posterior mean generated by the plain MCMC accelerated with the DL-based surrogate model is visually different from the posterior mean obtained from the numerical MCMC with the same number of samples. However, with additional 500 numerical samples, our hybrid approach gives a better result. A more quantitative comparison is included in Table 7 where the posterior expectation obtained from the hybrid MCMC algorithm is closer to the posterior expectation obtained from plain numerical MCMC with much higher computational cost.

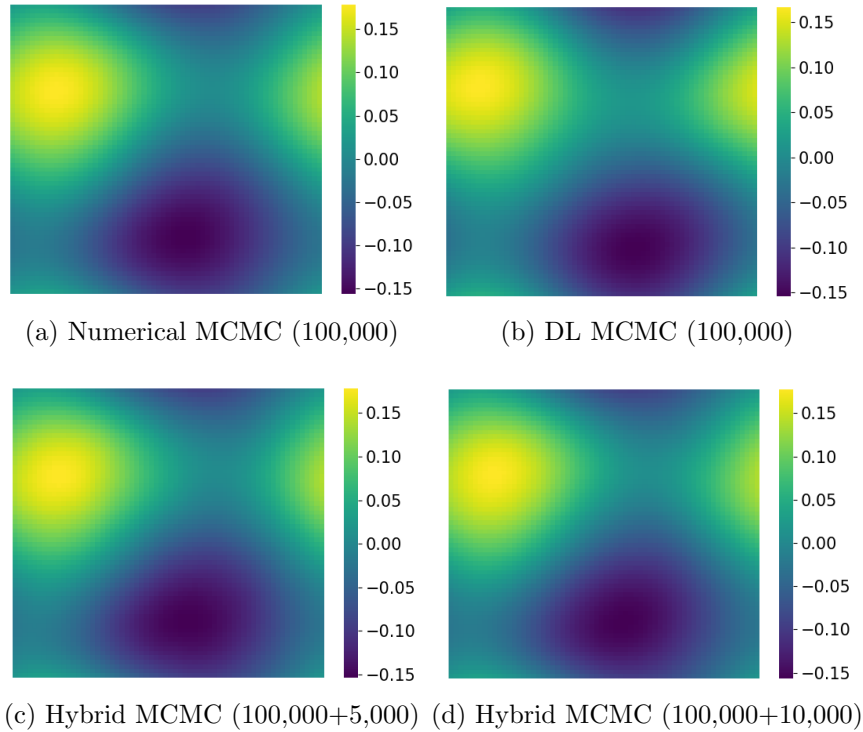


Figure 8: Expected mean of ω_0 from 8 runs of MCMC.

Method	Numerical MCMC	DL MCMC	Hybrid MCMC	Hybrid MCMC	Hybrid MCMC
Samples	100,000	100,000	100,000 + 1,000	100,000 + 5,000	100,000 + 10,000
L^2 difference from numerical MCMC	N.A.	0.000236	7.77e-05	3.26e-05	2.46e-05
L^∞ difference from numerical MCMC	N.A.	0.028963	0.015693	0.006429	0.004398
Compute time [s]	92343.7	456.4	923.4	4617.2	9234.4
Speed up	-	202.29x	100x	20x	10x

Table 7: Difference between the posterior expectation results of plain numerical MCMC and the posterior expectation results of the plain and hybrid DL-based MCMC with 2D Navier-Stokes equation

4. Conclusion

In this paper, we introduced a novel method, that we named hybrid two-level MCMC approach, to solve Bayesian inverse problems. In this method, we take advantage of the fast inference of DL surrogates and of the high accuracy of numerical models. In particular, we have theoretically shown the potential to solve Bayesian inverse problems accurately up to an estimator error $\mathcal{O}(h)$, by coupling one short MCMC chain generated by a high-fidelity numerical solver with mesh size h and another long MCMC chain generated with fast DL surrogates. We show the complete estimator error analysis and conclude that its theoretical bound is $\mathcal{O}(2^{-L})$ with one long base MCMC chain of $\mathcal{O}(2^{2L})$ number of DL surrogate samples and a short correction MCMC chain of $\mathcal{O}((1 + 2^\epsilon)^2)$ number of numerical samples, given the numerical forward model has an error rate of 2^{-L} and DL-based forward surrogate has an error rate of $2^{-L+\epsilon}$. In addition, we show that with a surrogate speedup rate s of one forward solve, the overall speedup of our hybrid algorithm is $\mathcal{O}(2^{2L} / \max((1/s)2^{2L}, (1 + 2^\epsilon)^2))$. This implies that the overall speedup depends on the performance of the surrogate model, more speedup can be expected with high accurate surrogate models due to less numerical samples needed for error correction. To validate the theoretical findings, we performed numerical experiments on the Poisson equation, the reaction-diffusion equation, and the Navier-Stokes equations. In all numerical experiments, we use both uniform priors and Gaussian priors. All results

of our numerical experiments are in agreement with the theoretical estimates proposed in this work. We note that the theoretical estimates proposed can also be used to understand the feasibility of using DL surrogates only (without hybridizing them with high-fidelity numerical solvers). More specifically, if the theoretical error estimates are already within the numerical error of a DL-only surrogate, then the use of the high-fidelity numerical solver is likely not yielding better accuracy. This theoretical result is particularly important, given the widespread use of DL surrogates in the field.

As a final note, this paper focuses on an hybrid approach for the MCMC method solving Bayesian inverse problem governed by PDEs; however, the same approach can in principle be applied to other Bayesian inverse problems not necessarily governed by PDEs, e.g. ODE governed Bayesian inverse problems, as well other methods such as filtering algorithms like the ensemble Kalman filter or sequential Monte Carlo methods.

Appendix A. Hybrid two-level MCMC with Gaussian Prior

In Section 2.3, we introduced our new hybrid two-level MCMC for Bayesian inverse problems with uniform priors. However, in several instances, it may be convenient to work with Gaussian priors. For completeness, in this section we discuss the hybrid two-level MCMC method for Gaussian prior. Similar to the case of uniform priors, we consider a forward model that predicts the states u of a physical system given parameter \mathbf{z} . In this case, the prior is Gaussian. Following the KL expansion (3) setup, we assume $\mathbf{b} := (\|\psi_j\|_{L^\infty(D)})_{j=1,2,\dots,n} \in \ell^1$. Then we define the measurable space (U, Γ_b) , with $\Gamma_b := \{z \in \mathbb{R}^n, \sum_{j=1}^n b_j |z_j| < \infty\} \in \mathcal{B}(\mathbb{R}^n)$, and U is the parameter space. We denote the standard Gaussian measure in \mathbb{R} by γ_1 . Hence, the prior can be defined as $\gamma = \bigotimes_{j=1}^n \gamma_1$ on $(\mathbb{R}^n, \mathcal{B}(\mathbb{R}^n))$, and it completes the probability space (U, Γ, γ) , noting that Γ_b has full Gaussian measure, i.e. $\gamma(\Gamma_b) = 1$.

Assumption Appendix A.1. *Let u be the solution of the forward problem in equation (2). We assume that $u \in V$, where V is a suitable vector space, e.g., a Sobolev space. The FEM approximation gives*

$$\|u(z) - u^\ell(z)\|_V \leq C \exp(c \sum_{j=1}^n b_j |z_j|) (1 + \sum_{j=1}^n \bar{b}_j |z_j|)^{2^{-l}}. \quad (\text{A.1})$$

The numerical error estimate in Assumption Appendix A.1 might not be true for all problems with Gaussian prior. It is problem-dependent. Yet, it is a typical error rate found in problems such as elliptic equations, diffusion problems, and parabolic problems with unknown coefficients, as investigated in [22, 23]. The right-hand side of Equation (A.1) differs from Assumption 2.2 made for a uniform prior, having an additional exponential term that depends on \mathbf{z} .

This specific form of approximation error is of significant interest for our two-level hybrid MCMC approach, because the exponential term in the error will lead to divergence of the method (in contrast to the uniform prior introduced in Section 2.3). However, with Fernique's theorem and an additional indication function to be presented below, we still can reach a similar posterior estimation error rate as the case in uniform prior. Using Assumption Appendix A.1, we can write the error between the DL-based surrogate

and the numerical discretization as follows

$$\begin{aligned} & \|u^{\text{num}}(z) - u^{\text{DL}}(z)\|_V \\ & \leq C(1 + 2^\epsilon) \exp\left(c \sum_{j=1}^n b_j |z_j| \right) \left(1 + \sum_{j=1}^n \bar{b}_j |z_j|\right) 2^{-l}, \end{aligned} \quad (\text{A.2})$$

$$\begin{aligned} & |\Phi^{\text{num}}(z; y) - \Phi^{\text{DL}}(z; y)| \\ & \leq C(1 + 2^\epsilon) \exp\left(c \sum_{j=1}^n b_j |z_j| \right) \left(1 + \sum_{j=1}^n \bar{b}_j |z_j|\right) 2^{-l}. \end{aligned} \quad (\text{A.3})$$

Next we derive the two level MCMC approach for Gaussian prior. In order to avoid the unboundedness from the exponential term, we make use of the following switching function

$$S(z) = \begin{cases} 1, & \text{if } \Phi^{\text{num}}(z, y) - \Phi^{\text{DL}}(z, y) \leq 0, \\ 0, & \text{otherwise.} \end{cases} \quad (\text{A.4})$$

With the switching function (A.4), we can write the expected quantity of interest as follows

$$\begin{aligned} & \left(\mathbb{E}^{\gamma^{\text{num}}} - \mathbb{E}^{\gamma^{\text{DL}}}\right) [Q] \\ & = \frac{1}{Z^{\text{num}}} \int_{\Gamma_{\mathbf{b}}} \exp(-\Phi^{\text{num}}) Q S(z) d\gamma - \frac{1}{Z^{\text{DL}}} \int_{\Gamma_{\mathbf{b}}} \exp(-\Phi^{\text{DL}}) Q S(z) d\gamma \\ & + \frac{1}{Z^{\text{num}}} \int_{\Gamma_{\mathbf{b}}} \exp(-\Phi^{\text{num}}) Q (1 - S(z)) d\gamma - \frac{1}{Z^{\text{DL}}} \int_{\Gamma_{\mathbf{b}}} \exp(-\Phi^{\text{DL}}) Q (1 - S(z)) d\gamma \\ & = \frac{1}{Z^{\text{num}}} \int_{\Gamma_{\mathbf{b}}} \exp(-\Phi^{\text{num}}) (1 - \exp(\Phi^{\text{num}} - \Phi^{\text{DL}})) Q S(z) d\gamma \\ & + \left(\frac{1}{Z^{\text{num}}} - \frac{1}{Z^{\text{DL}}}\right) \int_{\Gamma_{\mathbf{b}}} \exp(-\Phi^{\text{DL}}) Q S(z) d\gamma \\ & + \frac{1}{Z^{\text{DL}}} \int_{\Gamma_{\mathbf{b}}} \exp(-\Phi^{\text{DL}}) (\exp(\Phi^{\text{DL}} - \Phi^{\text{num}}) - 1) Q (1 - S(z)) d\gamma \\ & + \left(\frac{1}{Z^{\text{num}}} - \frac{1}{Z^{\text{DL}}}\right) \int_{\Gamma_{\mathbf{b}}} \exp(-\Phi^{\text{num}}) Q (1 - S(z)) d\gamma. \end{aligned} \quad (\text{A.5})$$

The constant $(1/Z^{\text{num}} - 1/Z^{\text{DL}})$, can be estimated via

$$\begin{aligned}
& \left(\frac{1}{Z^{\text{num}}} - \frac{1}{Z^{\text{DL}}} \right) = \\
& = \frac{1}{Z^{\text{num}} Z^{\text{DL}}} \int_{\Gamma_{\mathbf{b}}} (\exp(-\Phi^{\text{DL}}(z, y)) - \exp(-\Phi^{\text{num}}(z, y))) (S(z) + 1 - S(z)) d\gamma(z) = \\
& = \frac{1}{Z^{\text{num}} Z^{\text{DL}}} \int_{\Gamma_{\mathbf{b}}} \exp(-\Phi^{\text{num}}(z, y)) (\exp(\Phi^{\text{num}}(z, y) - \Phi^{\text{DL}}(z, y)) - 1) S(z) d\gamma(z) + \\
& + \frac{1}{Z^{\text{num}} Z^{\text{DL}}} \int_{\Gamma_{\mathbf{b}}} \exp(-\Phi^{\text{DL}}(z, y)) (1 - \exp(\Phi^{\text{DL}}(z, y) - \Phi^{\text{num}}(z, y))) (1 - S(z)) d\gamma(z) = \\
& = \frac{1}{Z^{\text{DL}}} \mathbb{E}^{\gamma^{\text{num}}} [(\exp(\Phi^{\text{num}}(z, y) - \Phi^{\text{DL}}(z, y)) - 1) S(z)] + \\
& + \frac{1}{Z^{\text{num}}} \mathbb{E}^{\gamma^{\text{DL}}} [(1 - \exp(\Phi^{\text{DL}}(z, y) - \Phi^{\text{num}}(z, y))) (1 - S(z))].
\end{aligned} \tag{A.6}$$

Combining equations (12), (A.5) and (A.6), we can derive the overall estimator of our hybrid two-level MCMC approach

$$\begin{aligned}
\mathbf{E}^{\text{hybrid}}(Q) &= \mathbf{E}^{\gamma^{\text{num}}} [A_1] + \mathbf{E}^{\gamma^{\text{num}}} [A_3] \cdot \mathbf{E}^{\gamma^{\text{DL}}} [A_4 + A_8] \\
&+ \mathbf{E}^{\gamma^{\text{DL}}} [A_2] + \mathbf{E}^{\gamma^{\text{DL}}} [A_5] \cdot \mathbf{E}^{\gamma^{\text{num}}} [A_6 + A_7] + \mathbf{E}^{\gamma^{\text{DL}}} [Q],
\end{aligned}$$

where the terms $A_1, A_2, A_3, A_4, A_5, A_6, A_7$ and A_8 are defined as follows

$$\begin{aligned}
A_1 &= (1 - \exp(\Phi^{\text{num}}(z) - \Phi^{\text{DL}}(z))) Q(z) S(z), \\
A_2 &= (\exp(\Phi^{\text{DL}}(z) - \Phi^{\text{num}}(z)) - 1) Q(z) (1 - S(z)), \\
A_3 &= (\exp(\Phi^{\text{num}}(z) - \Phi^{\text{DL}}(z)) - 1) S(z), \\
A_4 &= Q(z) \cdot S(z), \\
A_5 &= (1 - \exp(\Phi^{\text{DL}}(z) - \Phi^{\text{num}}(z))) (1 - S(z)) \\
A_6 &= \exp(\Phi^{\text{num}} - \Phi^{\text{DL}}) Q(z) S(z), \\
A_7 &= Q(z) (1 - S(z)), \\
A_8 &= \exp(\Phi^{\text{DL}}(z) - \Phi^{\text{num}}(z)) Q(z) (1 - S(z)).
\end{aligned}$$

We now perform the error analysis of our method, under the assumption of Gaussian priors. In analogy with what we have done for uniform priors in

Section 2.3, we decompose the error in three terms:

$$\mathbb{E}^{\gamma^y}[Q] - \mathbf{E}^{\text{hybrid}}[Q] = \text{I} + \text{II} + \text{III}, \quad (\text{A.7a})$$

$$\text{I} := \mathbb{E}^{\gamma^y}[Q] - \mathbb{E}^{\gamma^{\text{num}}}[Q], \quad (\text{A.7b})$$

$$\text{II} := \mathbb{E}^{\gamma^{\text{DL}}}[Q] - \mathbf{E}_{M_{\text{num}}}^{\gamma^{\text{DL}}}[Q], \quad (\text{A.7c})$$

$$\begin{aligned} \text{III} := & \mathbb{E}^{\gamma^{\text{num}}}[A_1] - \mathbf{E}_{M_{\text{num}}}^{\gamma^{\text{num}}}[A_1] + \mathbb{E}^{\gamma^{\text{num}}}[A_3] \cdot \mathbb{E}^{\gamma^{\text{DL}}}[A_4 + A_8] + \\ & - \mathbf{E}_{M_{\text{num}}}^{\gamma^{\text{num}}}[A_3] \cdot \mathbf{E}_{M_{\text{num}}}^{\gamma^{\text{DL}}}[A_4 + A_8] + \mathbb{E}^{\gamma^{\text{DL}}}[A_2] - \mathbf{E}_{M_{\text{num}}}^{\gamma^{\text{DL}}}[A_2] + \\ & + \mathbb{E}^{\gamma^{\text{DL}}}[A_5] \cdot \mathbb{E}^{\gamma^{\text{num}}}[A_6 + A_7] - \mathbf{E}_{M_{\text{num}}}^{\gamma^{\text{DL}}}[A_5] \cdot \mathbf{E}_{M_{\text{num}}}^{\gamma^{\text{num}}}[A_6 + A_7]. \end{aligned} \quad (\text{A.7d})$$

Similarly to Section 2.3, for each error term, we have the following error bounds

$$\text{I} < C2^{-L}, \quad (\text{A.8a})$$

$$\text{II} < M_{\text{DL}}^{-1/2}, \quad (\text{A.8b})$$

$$\text{III} < C(1 + 2^\epsilon)^2 M_{\text{num}}^{-1} 2^{-2L}. \quad (\text{A.8c})$$

Therefore, choosing $M_{\text{DL}} = 2^{2L}$ and $M_{\text{num}} = (1 + 2^\epsilon)^2$, allows us to obtain a theorem for the overall error estimate.

Theorem Appendix A.1. *With $M_{\text{DL}} = C2^{2L}$ and $M_{\text{num}} = C(1 + 2^\epsilon)^2$, we have the following theoretical error estimate of our hybrid two-level MCMC approach under Gaussian priors*

$$\mathbf{E}[|\mathbb{E}^{\gamma^y}[Q] - \mathbf{E}^{\text{hybrid}}[Q]|] \leq C2^{-L}. \quad (\text{A.9})$$

From Theorem Appendix A.1, we see the same results as the one from Theorem 2.1 derived from uniform prior setup. The theorem and the preceding assumptions are typically valid for log-normal priors with elliptic, diffusion, and parabolic equations. The proof for the two-dimensional Navier-Stokes equation is not available to the best of our knowledge. However, some experimental results also show the theorem for multilevel MCMC with Gaussian prior works for the two-dimensional Navier-Stokes equation [49].

Appendix B. Forward numerical solvers and deep learning surrogate models

We present the details of the forward numerical solvers used for solving each of the problems presented in Section 3, along with the corresponding DL surrogate.

Appendix B.1. Poisson equation

The Poisson equation 25 in Section 3.1 is solved with the finite element package Fenicsx [4], whereby first-order Lagrange finite elements are used to discretize the equation. The mesh adopted is constituted of 32×32 elements as shown in Figure 2a. A direct LU solver from MUMPS backend is used to solve the assembled linear system on CPU.

For the simple uniform prior setup in Section 3.1.1, we choose a fully connected ReLU neural network to learn the forward mapping from the 4000 generated training samples. The input field of 33×33 is flattened and feed in as input data. Two hidden layer is included each with a number of 512 nodes. The neural network is implemented with PyTorch. The trained neural network is used as the DL-based surrogate model in the experiment.

For the Gaussian prior setup in Section 3.1.2, we choose a convolutional neural network (CNN) to be our DL-based surrogate model. The CNN model consists of 3 encoding layers, 1 fully connected layer, and 3 decoding layers. There are 8 kernels in each convolutional layer, and the kernel size is $(3, 3)$ with stride size $(2, 2)$.

Appendix B.2. Reaction-diffusion equation

To solve the reaction diffusion equation (27) in Section 3.2, we also use the finite element package Fenicsx [4], whereby first-order Lagrange finite elements are used to discretize the equation. The resulting nonlinear system is solved with the Newton solver from the PETSC backend. Each linearized Newton iteration step is solved with LU direct solver with MUMPS backend.

For the DL-based surrogate model, we choose message passing graph neural network (MPGNN) for the uniform prior case. We refer to the Graph-PDE architecture [25] as our reference. Instead of training the MPGNN for a time dependent problem, here we train the neural network for a time independent problem. Two fully connected multilayer neural networks are used for the message passing and state update. There are two hidden layers each with 64 nodes in both the message passing and state update neural

networks. The hidden state vector output from the message passing neural network is of size 64. A Dirichlet boundary condition is also imposed on the MPGNN. Five layers of MPGNN are stacked in the model used in the experiments. The MPGNN is trained with 2000 training samples with Adam optimizer and trained for 10000 epoches.

We then choose U-net proposed in [43] for the Gaussian prior experiment. It is well-known for its outstanding performance in multi-scale physical problems. The U-net consists of 3 layers, each with dimensions of 32×32 , 16×16 , and 8×8 . For each convolutional layer we have 8 kernel with size $(3, 3)$ and stride size $(1, 1)$.

Appendix B.3. Navier-Stokes equations in the vorticity form

To solve the Navier-Stokes equations 28 in Section 3.3, we coded a simple numerical pseudo-spectral solver with PyTorch, which is accelerated on GPU. A total of 64×64 collocation points are used for the experiments. The interested reader can refer to [41] for details of the spectral method implemented.

For the DL-based surrogate model, we first choose the DeepONet [34] as the deep learning model for the uniform prior experiment. Two fully connected multilayer neural networks are used as the branch net and trunk net. For both the branch net and trunk net, both have two hidden layers with 64 nodes in the neural network. The DeepONet model is trained with 4000 samples of numerical data for 10000 epoches.

Then we choose the Fourier Neural Operator for the Gaussian prior experiment, as it demonstrated its ability to learn the dynamics of the Navier-Stokes equation in [33] and has also been shown to be used in a Bayesian inversion problem setup with MCMC. Specifically, the two-dimensional Fourier neural operator with tensor layers is used. There are 12 modes for height and width, 8 hidden channels, and 4 layers in the FNO we used in this experiment. The neural network is trained with 2000 training data for 10000 epochs.

References

- [1] Zeyuan Allen-Zhu, Yuanzhi Li, and Zhao Song, *A convergence theory for deep learning via over-parameterization*, Proceedings of the 36th international conference on machine learning, 201909, pp. 242–252.
- [2] Richard C. Aster, Brian Borchers, and Clifford H. Thurber, *Parameter estimation and inverse problems*, Second, Elsevier/Academic Press, Amsterdam, 2013. MR3285819
- [3] Y. Bahri, E. Dyer, J. Kaplan, J. Lee, and U. Sharma, *Explaining neural scaling laws*, Proceedings of the National Academy of Sciences **121** (2024).
- [4] Igor A Barrata, Joseph P Dean, Jørgen S Dokken, Michal Habera, Jack HALE, Chris Richardson, Marie E Rognes, Matthew W Scroggs, Nathan Sime, and Garth N Wells, *Dolfinx: The next generation fenics problem solving environment* (2023).
- [5] Dietrich Braess, *Finite elements*, Third, Cambridge University Press, Cambridge, 2007. Theory, fast solvers, and applications in elasticity theory, Translated from the German by Larry L. Schumaker. MR2322235
- [6] Steve Brooks, Andrew Gelman, Galin Jones, and Xiao-Li Meng, *Handbook of markov chain monte carlo*, CRC press, 2011.
- [7] Erhan Çinlar, *Probability and stochastics*, Graduate Texts in Mathematics, vol. 261, Springer, New York, 2011. MR2767184
- [8] C.D. Cantwell, D. Moxey, A. Comerford, A. Bolis, G. Rocco, G. Mengaldo, D. De Grazia, S. Yakovlev, J.-E. Lombard, D. Ekelschot, B. Jordi, H. Xu, Y. Mohamied, C. Eskilsson, B. Nelson, P. Vos, C. Biotto, R.M. Kirby, and S.J. Sherwin, *Nektar++: An open-source spectral/hp element framework*, Computer Physics Communications **192** (2015), 205–219.
- [9] Lianghao Cao, Thomas O’Leary-Roseberry, Prashant K. Jha, J. Tinsley Oden, and Omar Ghattas, *Residual-based error correction for neural operator accelerated infinite-dimensional bayesian inverse problems*, Journal of Computational Physics **486** (2023), 112104.
- [10] Tianping Chen and Hong Chen, *Universal approximation to nonlinear operators by neural networks with arbitrary activation functions and its application to dynamical systems*, IEEE Transactions on Neural Networks **6** (1995), no. 4, 911–917.
- [11] S. L. Cotter, M. Dashti, J. C. Robinson, and A. M. Stuart, *Bayesian inverse problems for functions and applications to fluid mechanics*, Inverse Problems **25** (2009), no. 11, 115008, 43. MR2558668
- [12] Oliver Dorn and Rossmary Villegas, *History matching of petroleum reservoirs using a level set technique*, Inverse Problems **24** (2008), no. 3, 035015, 29. MR2421969
- [13] Simon Du, Jason Lee, Haochuan Li, Liwei Wang, and Xiyu Zhai, *Gradient descent finds global minima of deep neural networks*, International conference on machine learning, 2019, pp. 1675–1685.

- [14] Y. Efendiev, T. Hou, and W. Luo, *Preconditioning Markov chain Monte Carlo simulations using coarse-scale models*, SIAM J. Sci. Comput. **28** (2006), no. 2, 776–803. MR2231730
- [15] Yalchin Efendiev, Bangti Jin, Michael Presho, and Xiaosi Tan, *Multilevel Markov chain Monte Carlo method for high-contrast single-phase flow problems*, Commun. Comput. Phys. **17** (2015), no. 1, 259–286. MR3372290
- [16] Alexandre Ern and Jean-Luc Guermond, *Theory and practice of finite elements*, Applied Mathematical Sciences, vol. 159, Springer-Verlag, New York, 2004. MR2050138
- [17] Michael B. Giles, *Multilevel Monte Carlo path simulation*, Oper. Res. **56** (2008), no. 3, 607–617. MR2436856
- [18] Yinnian He, *The Euler implicit/explicit scheme for the 2D time-dependent Navier-Stokes equations with smooth or non-smooth initial data*, Math. Comp. **77** (2008), no. 264, 2097–2124. MR2429876
- [19] Joel Hestness, Sharan Narang, Newsha Ardalani, Gregory Diamos, Heewoo Jun, Hassan Kianinejad, Md Patwary, Mostofa Ali, Yang Yang, and Yanqi Zhou, *Deep learning scaling is predictable, empirically*, arXiv preprint arXiv:1712.00409 (2017).
- [20] John G. Heywood and Rolf Rannacher, *Finite-element approximation of the nonstationary Navier-Stokes problem. IV. Error analysis for second-order time discretization*, SIAM J. Numer. Anal. **27** (1990), no. 2, 353–384. MR1043610
- [21] Viet Ha Hoang, Jia Hao Quek, and Christoph Schwab, *Analysis of a multilevel Markov chain Monte Carlo finite element method for Bayesian inversion of log-normal diffusions*, Inverse Problems **36** (2020), no. 3, 035021, 46. MR4069815
- [22] ———, *Multilevel Markov chain Monte Carlo for Bayesian inversion of parabolic partial differential equations under Gaussian prior*, SIAM/ASA J. Uncertain. Quantif. **9** (2021), no. 2, 384–419. MR4246090
- [23] Viet Ha Hoang and Christoph Schwab, *Convergence rate analysis of mcmc-fem for bayesian inversion of log-normal diffusion problems*, Research reports/seminar for applied mathematics, 2016.
- [24] Viet Ha Hoang, Christoph Schwab, and Andrew M. Stuart, *Complexity analysis of accelerated MCMC methods for Bayesian inversion*, Inverse Problems **29** (2013), no. 8, 085010, 37. MR3084684
- [25] Valerii Iakovlev, Markus Heinonen, and Harri Lähdesmäki, *Learning continuous-time pdes from sparse data with graph neural networks*, International conference on learning representations, 2020.
- [26] Antony Jameson and D Caughey, *A finite volume method for transonic potential flow calculations*, 3rd computational fluid dynamics conference, 1977, pp. 635.
- [27] Arnulf Jentzen, Benno Kuckuck, Ariel Neufeld, and Philippe von Wurstemberger, *Strong error analysis for stochastic gradient descent optimization algorithms*, IMA Journal of Numerical Analysis **41** (202005), no. 1, 455–492, available at <https://academic.oup.com/imajna/article-pdf/41/1/455/35970895/drz055.pdf>.

- [28] Pengzhan Jin, Lu Lu, Yifa Tang, and George Em Karniadakis, *Quantifying the generalization error in deep learning in terms of data distribution and neural network smoothness*, *Neural Networks* **130** (2020), 85–99.
- [29] Jari Kaipio and Erkki Somersalo, *Statistical and computational inverse problems*, *Applied Mathematical Sciences*, vol. 160, Springer-Verlag, New York, 2005. MR2102218
- [30] George Karniadakis and Spencer J Sherwin, *Spectral/hp element methods for computational fluid dynamics*, Oxford University Press, USA, 2005.
- [31] Moshe Leshno, Vladimir Ya. Lin, Allan Pinkus, and Shimon Schocken, *Multilayer feedforward networks with a nonpolynomial activation function can approximate any function*, *Neural Networks* **6** (1993), no. 6, 861–867.
- [32] Randall J. LeVeque, *Finite volume methods for hyperbolic problems*, *Cambridge Texts in Applied Mathematics*, Cambridge University Press, Cambridge, 2002. MR1925043
- [33] Zongyi Li, Nikola Borislavov Kovachki, Kamyar Azizzadenesheli, Burigede Liu, Kaushik Bhattacharya, Andrew M. Stuart, and Anima Anandkumar, *Fourier neural operator for parametric partial differential equations*, 9th international conference on learning representations, ICLR 2021, virtual event, austria, may 3-7, 2021, 2021.
- [34] Lu Lu, Pengzhan Jin, Guofei Pang, Zhongqiang Zhang, and George Em Karniadakis, *Learning nonlinear operators via deeponet based on the universal approximation theorem of operators*, *Nature Machine Intelligence* **3** (2021), no. 3, 218–229.
- [35] Lu Lu, Xuhui Meng, Shengze Cai, Zhiping Mao, Somdatta Goswami, Zhongqiang Zhang, and George Em Karniadakis, *A comprehensive and fair comparison of two neural operators (with practical extensions) based on fair data*, *Computer Methods in Applied Mechanics and Engineering* **393** (2022), 114778.
- [36] Romit Maulik, Vishwas Rao, Jiali Wang, Gianmarco Mengaldo, Emil Constantinescu, Bethany Lusch, Prasanna Balaprakash, Ian Foster, and Rao Kotamarthi, *Efficient high-dimensional variational data assimilation with machine-learned reduced-order models*, *Geoscientific Model Development* **15** (2022), no. 8, 3433–3445.
- [37] Gianmarco Mengaldo, David Moxey, Michael Turner, Rodrigo Costa Moura, Ayad Jassim, Mark Taylor, Joaquim Peiró, and Spencer J Sherwin, *Industry-relevant implicit large-eddy simulation of a high-performance road car via spectral/hp element methods*, *SIAM Review* **63** (2021), no. 4.
- [38] S. Mishra, Ch. Schwab, and J. Šukys, *Multi-level Monte Carlo finite volume methods for nonlinear systems of conservation laws in multi-dimensions*, *J. Comput. Phys.* **231** (2012), no. 8, 3365–3388. MR2897628
- [39] Nicola Parolini and Alfio Quarteroni, *Mathematical models and numerical simulations for the america’s cup*, *Computer Methods in Applied Mechanics and Engineering* **194** (2005), no. 9-11, 1001–1026.
- [40] Philipp Petersen and Felix Voigtlaender, *Optimal approximation of piecewise smooth functions using deep relu neural networks*, *Neural Networks* **108** (2018), 296–330.

- [41] Roger Peyret, *Spectral methods for incompressible viscous flow*, Vol. 148, Springer, 2002.
- [42] M. Raissi, P. Perdikaris, and G. E. Karniadakis, *Physics-informed neural networks: a deep learning framework for solving forward and inverse problems involving nonlinear partial differential equations*, J. Comput. Phys. **378** (2019), 686–707. MR3881695
- [43] Olaf Ronneberger, Philipp Fischer, and Thomas Brox, *U-net: Convolutional networks for biomedical image segmentation*, Medical image computing and computer-assisted intervention – miccai 2015, 2015, pp. 234–241.
- [44] William C Skamarock, Joseph B Klemp, Jimy Dudhia, David O Gill, Zhiqian Liu, Judith Berner, Wei Wang, Jordan G Powers, Michael G Duda, Dale M Barker, and Xiang-Yu Huang, *A description of the advanced research wrf version 4*, Technical Report NCAR/TN-556+STR, National Center for Atmospheric Research, 2019.
- [45] A. M. Stuart, *Inverse problems: a Bayesian perspective*, Acta Numer. **19** (2010), 451–559. MR2652785
- [46] Albert Tarantola, *Inverse problem theory and methods for model parameter estimation*, Society for Industrial and Applied Mathematics (SIAM), Philadelphia, PA, 2005. MR2130010
- [47] Umberto Villa, Noemi Petra, and Omar Ghattas, *HIPPYlib: An Extensible Software Framework for Large-Scale Inverse Problems Governed by PDEs: Part I: Deterministic Inversion and Linearized Bayesian Inference*, ACM Trans. Math. Softw. **47** (April 2021), no. 2.
- [48] Jinchao Xu, *Finite neuron method and convergence analysis*, Communications in Computational Physics **28** (2020), no. 5, 1707–1745.
- [49] Juntao Yang and Viet Ha Hoang, *Multilevel Markov Chain Monte Carlo for Bayesian inverse problem for Navier-Stokes equation*, Inverse Probl. Imaging **17** (2023), no. 1, 106–135. MR4523340